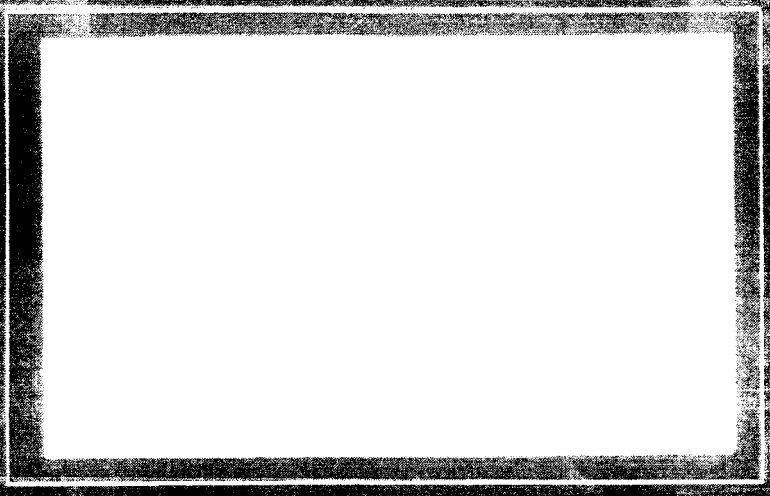



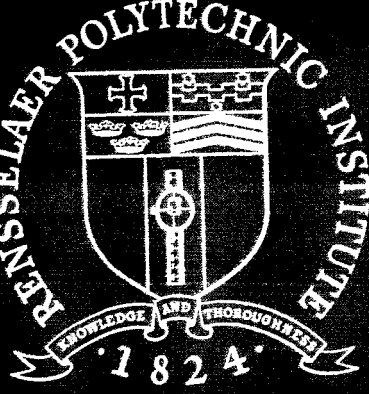


# Rensselaer Polytechnic Institute

## Troy, New York

UNPUBLISHED PRELIMINARY DATA

PROGRESS REPORT
Covering Period from 15 Sept. 1963
to 15 March 1964

# RADIATION DAMAGE TO SEMICONDUCTORS BY HIGH-ENERGY ELECTRON AND PROTON RADIATION

Sponsored by the National Aeronautics and Space Administration
under Grant NsG-290

Department of
Nuclear Engineering and Science
Rensselaer Polytechnic Institute
Troy, New York

## INTRODUCTION AND SUMMARY

The results given in this progress report have been gathered from the research efforts of the following personnel:

Dr. John C. Corelli and six graduate students, Li-Jen Cheng, John Becker, John Fischer*, Orrin H. Merrill, Charles Taylor and Arne Kalma. The graduate students are half-time research assistants spending a minimum of twenty hours per week on research work. The progress of research is discussed as the need arises either weekly or bi-weekly with Dr. H.B.Huntington of the physics department.

Only research performed from 15 September 1963 to 15 March 1964 is included in this report. The general topics covered are 1) Infrared studies on 40-Mev Electron irradiated silicon (both floating - zone and crucible grown) 2) Cold temperature (95-100$^{o}$K) irradiation of Ge and Si by 40-Mev electrons (conductivity and Hall effect) 3) 24-110 Mev proton bombardment at 300$^{o}$K of germanium using carrier lifetime, conductivity and Hall effect as probes of the radiation damage 4) 12-52 Mev electron bombardment at 300$^{o}$K of germanium and silicon (conductivity and Hall effect).

---

*NDEA Fellow no salary charged to NASA Grant NsG-290

TABLE OF CONTENTS

# COLD TEMPERATURE (90-100°K) IRRADIATION OF GERMANIUM AND SILICON WITH 40 MEV ELECTRONS

## Introduction

Bridge-type samples suitable for Hall coefficient and conductivity measurements, of n- and p-type germanium and silicon were irradiated with 26 to 45 Mev electrons using the cryostat and techniques described previously*. In the results to be presented here the samples were irradiated at cold temperatures in the range 90 to 100°K, with subsequent annealing from 95°K to 330°K. These cold temperatures were achieved with liquid nitrogen coolant in the cryostat. However, the cryostat is capable of running at liquid helium temperatures and we are currently preparing to irradiate low resistivity silicon and germanium ($\rho \cong 0.1\,\Omega$-cm) at low temperature during a Linac run April 1, 1964. In these liquid helium experiments we expect to reach temperatures below the 35°K annealing peak found by MacKay and Klontz[1] in 1 Mev electron-irradiated germanium.

## Experimental Procedures

Before irradiation the temperature dependence of the Hall coefficient, $R_H$ and conductivity, $\sigma$, of each sample was measured. The samples were measured in the dark in

---

*See RPI Progress Report Covering Period from 15 March 1963 to 15 September 1963

our particular cryostat with no provision for the introduction of even modest amounts of light. During irradiation the beam was always turned off when measurements were performed. After completion of the irradiation the cryostat was moved out of the accelerator target room with the samples kept cold (90-100°K). The annealing experiments were performed by warming the samples from 90 to 100°K up to successively higher temperature, measuring $R_H$ and $\sigma$ as a function of time and then cooling down to 90 to 100°K and remeasuring $R_H$ and $\sigma$. This procedure was continued until about 300-320°K was reached. For all experiments the post-irradiation annealing measurements were finished 8 to 12 hours after completion of the bombardment. It is important to keep the above mentioned procedures in mind particularly in view of the trapping effects we observed in both p-type silicon and germanium. Unless otherwise stated the electrons were incident on the sample in the <111> direction during bombardment.

## Results and Discussion

In this report we have only included the analyzed experimental results completed at this time. Further analysis is in progress and when completed to a point where better interpretation is possible then a more comprehensive paper will be published.

The recovery of the Hall coefficient of a 3.5 ohm-cm arsenic-doped germanium sample is shown in Fig. 1. The sample was irradiated with 46-Mev electrons at 93°K to $2.6 \times 10^{14}$ e/cm$^2$. The increase in $R_H$ indicates that acceptor type defects are introduced which remove carriers from the conduction band. The measured carrier removal rate was 1.9 cm$^{-1}$ and was obtained from a plot of $\frac{1}{R_H e}$ vs integrated electron flux. After irradiation the first warmup run is shown as the uppermost curve in Fig. 1. Successively higher temperatures are shown by the series of curves proceeding from the top to the bottom of Fig. 1. We observe continuous annealing of the defects formed by the irradiation from 93°K up to room temperature. The break in the last two annealing curves at $\sim$ 200°K is the only handle we have on a "stable" defect. This temperature dependence of carrier concentration yields an activation energy for this "stable" defect level lying $0.26 \pm 0.02$ ev below the bottom of the conduction band. It is important to observe from Fig. 1 that in addition to the shallow level at 0.26 ev a deep level (unresolvable) at $> 0.35$ ev below conduction band edge is still operative in removing carriers from the conduction band. The calculational procedure given by Kitovski[2] et al., has been used to determine the position of the shallow level.

The annealing behavior shown in Fig. 1 is in marked difference to what has been observed by Brown[3] in 0.5 Mev electron irradiation of comparable resistivity arsenic-doped germanium. The defects introduced at 0.5 Mev are in fact near threshold events; Brown[4] measured the electron energy necessary to just displace a germanium atom, which was $\sim$0.400 Mev. Brown observed no annealing from 79°K up to 300°K after an irradiation dose sufficient to lower the carrier concentration by only 27%. The defects introduced into our sample, Fig. 1, have changed the carrier concentration by a factor of 10, and after the annealing we have approximately 65% lower carrier concentration. This is still a factor 2.4 larger defect concentration than that Brown[3] shows in Fig. 3 of his paper. These facts and close inspection of Fig. 1 imply that the annealing behavior itself is dependent perhaps critically upon the number of defects introduced. One can probably assume that the defects created by 44 Mev electrons in our experiment are not as simple nor in general not as isolated as for the 0.5 Mev case, and it may be that the defects annealing in Fig. 1 are the breakup of aggregates of vacancies, interstitials and impurity atoms.

An important underlying factor of the defects is the appearance of energy levels at 0.26 $\pm$ 0.02 ev and the deep

level. These levels have been observed in all radiation damage experiments involving n-type germanium. To list a few 20-130 Mev protons Corelli[5] et al., 1.7 Mev gamma rays Crawford and Cleland,[6] reactor neutrons Crawford and Cleland,[6] 10 Mev deuterons and 4.5 electrons Fan and Lark-Horovitz[7] and 22 Mev protons, Breckenridge and Gross.[8] It therefore appears that a study of the configuration (say by spin resonance, or some other method not utilized thus far in research) of the defect responsible for the energy levels would be extremely significant to the general problem of understanding the radiation damage in germanium.

Before ending the remarks on the n-type germanium we observe that one can attribute practically the entire damage predominantly to carrier trapping since there is little effect on the Hall mobility as is shown in Fig. 2. The remarkably small decrease in mobility (Fig. 2) indicates that defects introduced cause little or no change in the number of ionized impurity centers which are the main causes of the electron scattering. The results of Figs. 1 and 2 strongly suggest that the defects which annealed out are composed of mostly neutral impurities.

The temperature dependence of the carrier concentration and conductivity of indium-doped 1 and 10 ohm-cm p-type

germanium after irradiation by 36 Mev electrons to 2.4 X $10^{15}$ $e/cm^2$ at $\sim$ 100°K is shown in Figs. 3, 4, 5, and 6. The carrier removal rates measured were 0.58 $cm^{-1}$ for the 1 ohm-cm sample and 0.33 $cm^{-1}$ for the 10 ohm-cm sample. Note these are what we may call the average removal rate of holes as measured from the slope of the linear portion of the $1/R_H e$ vs integrated flux curves early in the irradiation. This interpretation must be qualified by the fact that for the 10$\Omega$-cm sample we find after annealing an addition of holes (see Fig. 5). We shall discuss this point briefly later and show how close agreement is found with results of Fig. 5 and other experiments we have performed.

From Figs. 3 and 5 and the carrier concentration vs flux measurements one finds a relatively low donor introduction rate in p-type germanium during irradiation with 36 Mev electrons at 100°K. After warmup to $\sim$120°K many more donors are present as can be seen by the rapid rise in resistivity and Hall coefficient at $\frac{1000}{T} \cong 8.5$. The 10$\Omega$-cm p-type germanium sample exhibited the rise in $R_H$ even at the irradiation temperature. In fact the increase in $R_H$ for the 10$\Omega$-cm sample of Fig. 5 was so large that we lost sensitivity on the measuring instrument (only $10^8$

ohms input impedance) and were not able* to follow the Hall voltage measurements. It appears that the temperature at which $R_H$ becomes larger depends on the initial minority carrier concentration.

Temperature dependence of carrier concentration giving results similar to those found in Figs. 3-6 have been observed by Brown[3] in 1-Mev electron irradiated indium-doped germanium with resistivity of $\sim 5\,\Omega$-cm. However the increase in donor concentration observed by Brown is not as large as that shown in Figs. 3 to 6. In electron irradiated ($E < 5$ Mev) p-type germanium at $T < 90^{\circ}K$ effects similar to those shown in Figs. 3 to 6 have been observed by Dr. John MacKay[9] and his colleagues at Purdue University.

The phenomena shown in Figs. 3-6 can be described as an inverse annealing and has been interpreted by Brown[3] as due to minority carrier (electron) trapping on the defect centers. At $T \lesssim 90^{\circ}$ Brown[3] finds that "the time constant for establishing equilibrium (once the traps are filled with electrons) as they will be from ionization by the electron beam is extremely long, of the order of 1 to 2 days at least." We find the same behavior at $105^{\circ}K$.

---

*Due to an unforeseen circumstance our vibrating reed electrometer ($10^{14}$ ohms input impedance) was being used on another experiment in a different building at RPI.

By warming up to say 120-180°K the traps "unload" the electrons and reach equilibrium more rapidly. We measured the time dependence for unloading the trapped electrons at 118°K. These results are shown in Fig. 7 for both the 1 and 10 Ω-cm indium-doped germanium samples. At this temperature we note that the time constant for establishing equilibrium is about one hour. Analysis of the "inverse annealing results" of Fig. 7 have been made using the rate equation. We find that second order kinetics yields only a fair fit to the data implying that a more complex process may be occurring. We have also tried to fit the annealing data to a first order reaction and to an order of 1.5. For these cases the fit is not satisfactory. Note, that we do not observe any annealing below temperatures where electrons are unloaded similar to the results of Brown[3].

The annealing that took place at 180-200°K was so rapid that accurate time dependent runs could not be made. This annealing stage at $\sim$ 190°K was observed by Brown[3] and his co-workers, and was also observed by us previously in 1 ohm-cm p-type germanium and given in the last progress report.

After annealing 10 Ω-cm p-type germanium to room temperature (see Figs. 5 and 6) we find an unannealed

damage residue consisting of the net addition of holes, lower $\rho$ and $R_H$. This is exactly what we observed earlier in 10 ohm-cm p-type germanium irradiated at room temperature by 40 Mev electrons. The slopes in the $R_H$ vs 1000/T curve 10$\Omega$-cm p-type germanium Fig. 5 are indicative of trapping levels 0.26 and possibly at $\sim$ 0.14 ev above the valance band. We can now conclude that for 40 Mev electron irradiation at $\sim 90^{o}$K both donor and acceptor levels are introduced while irradiation above the annealing stage at $\sim 190^{o}$K introduces predominantly acceptor-type defects in moderately high resistivity (10$\Omega$-cm) p-type germanium.

Trapping effects similar to the case of p-type germanium have also been observed by our group in cold temperature irradiation of p-type silicon. Fig. 8 shows the annealing of the Hall coefficient of a 10 ohm-cm boron-doped p-type silicon sample (floating zone) after a $97^{o}$K irradiation by 45 Mev. electrons. The irradiation decreased the hole concentration by a factor $\sim 10^3$ with a measurement of the average carrier removal rate yielding a value 1.0 $cm^{-1}$. Fig. 9 shows the annealing of resistivity for this sample. After irradiation and immediately upon warmup both the resistivity and Hall coefficient increased abruptly, then annealed in what appear to be two temperature stages (see Figs. 8 and 9), the first at $\sim 120^{o}$K and a second stage at $\sim 190^{o}$K. Similar temperature dependent results

to those shown in Figs. 8 and 9 were observed in an irradiation of 1 ohm-cm boron-doped p-type silicon (floating zone.)

Previous irradiation of 10 ohm-cm arsenic-doped n-type silicon (floating-zone) with 40 Mev electrons at $\sim$100°K yielded a carrier removal rate of 0.3 $cm^{-1}$ indicating that defects are produced more efficiently in p-type than n-type silicon when the defects are produced at cold temperatures. The opposite is true when the irradiation is performed at room temperature (see our previous progress report.)

The results indicate that at low temperature the defects in p-type silicon are more mobile than in n-type silicon. The slopes of $R_H$ vs temperature curve in Fig. 8 after annealing suggest the presence of one and possibly two energy levels above the valence band at $\sim$ 0.16 and$\sim$0.1 ev. However we can not make definitive statements on the 0.1 ev level until more experiments are performed.

Before concluding this section of the report we wish to give results found for both n and p-type silicon. We have found for both p and n-type silicon that the Hall mobility <u>increased</u> after irradiation around 100°K. This effect is not understood at present; more research is necessary to explore this effect further.

# INFRARED STUDIES ON 40-MEV ELECTRON-IRRADIATED SILICON*

## Introduction

The use of infrared spectroscopy for the study of radiation induced defects in silicon has been shown to be an important probe by many workers[10-15] in recent years. In the past, the defects introduced in silicon by reactor neutrons, 9.6 Mev deuterons and electrons of energy less than 4.5 Mev were observed to give rise to new infrared absorption bands in silicon in the wavelength region 1.8 to 20.5 microns. However, no previous studies on infrared bands induced in silicon by high-energy electrons (12-60 Mev) were reported. In an earlier progress report (1 September 1962 - 15 March 1963) to NASA we reported that silicon (floating-zone) of 1 and 10 ohm-cm resistivity irradiated with 50-Mev electrons to total integrated fluxes of $10^{16}$ - $10^{17}$ $e/cm^2$ exhibited no detectable radiation-induced defect absorption bands (at room temperature) in the wavelength range 1-40 microns. From the previous work of Fan and Ramdas[10,11,13] it was known that integrated fluxes of $10^{18}$ to $10^{19}$ particles/$cm^2$ are necessary before one can easily detect new bands. Because relatively large fluxes were required and sufficient personnel active with the program were lacking at that time (October 1962) the infrared work was temporarily stopped.

---

*We acknowledge the assistance of Dr. Kent Eisentrant of the RPI Chemistry Department for his invaluable help in making the infrared measurements.

During the past year our experimental results on the defect characteristics (as measured by the electrical properties) of both germanium and silicon irradiated with 10-60 Mev electrons and 20-130 Mev protons have shown a close similarity to what has been observed with other energies and particles, e.g. $Co^{60}$ gamma rays (1.7 Mev), low energy electrons ($<$5 Mev), and reactor neutrons. The similarities were detected specifically from the localized energy levels in the forebidden energy gap giving rise to both donor and a acceptor states, and annealing in p-type germanium at 190°K after a 95°K irradiation. These are perhaps the most pertinent defect properties which we detected and had been observed previously at low bombarding energies. It became apparent on account of this similarity in the radiation damage that we should search in more detail for radiation-induced infrared defect absorption bands. In this report we shall give the first results of our current infrared experiments, and where possible point out once again similarities in defect absorption bands produced by high-energy electrons and those observed by others[10-15].

Experimental Methods

Discs of oxygen-free floating zone silicon samples 20-26 mm in diameter and thickness ranging from 2.5 mm to 9 mm were cut from ingots purchased from Merck Co. Inc. The samples were etched, lapped and finally polished to a mirror-like finish. Oxygen-containing pulled silicon of 25 mm diameter and

2.5 mm thickness were kindly supplied to us by NASA*. The exact thickness of each sample is shown in Figs. 10 and 11 and in Table I.

In order to accumulate high doses, 1-2 X $10^{18}$ e/$cm^2$, in short irradiation times without excessive heating, the samples were mounted in a metal box through which water flowed at 5 gpm. The sample temperature was monitored continuously during bombardment by a copper-constantan thermocouple pressed to the sample by a screw arrangement. With this setup the Linac was operated at $\sim$ 40 Mev delivering $\sim 100\,\mu$ amp/$cm^2$ on the sample. The electron beam was directed in the $\langle 111 \rangle$ direction for all samples irradiated. The sample temperature during irradiation never exceeded 40°C.

The infrared spectra before and after irradiation were measured using a Perkin-Elmer model 421 prism spectrometer with a CsBr interchange. The model 421 was used to measure the infrared spectra from 2-40 microns. A second spectrometer, Perkin-Elmer model 12 was used to measure the infrared spectra from 0.7 to 2.5 microns. The measurements were made at both 295°K and at $\sim$85°K. The low temperature measurements were

---

*The completely prepared oxygen-containing silicon (polished etched etc.) samples were given to us for our experiment by the Instrument Research Division of the NASA Langley Research Center, Hampton, Va.

made using an evacuated cell* with NaCl or CsBr windows. The sample was cooled by mounting it to copper rings in contact with liquid nitrogen.

Results and Discussion

The sample impurity, resistivity, incident electron energy, total integrated flux and thickness for each of the four silicon samples studied are given in Table II. After irradiation all samples were nearly intrinsic as determined from thermoelectric power measurements. Carrier concentrations were not measured on these samples before and after irradiation.

Figure 10 shows the infrared spectra measured at 85°K and 295°K in the range 1-3 microns for oxygen-containing (crucible grown) and floating zone n-type silicon samples after electron irradiation. The radiation-induced defect absorption band at 1.8 microns shifts toward shorter wavelengths and is sharpened when the sample is cooled to 85°K. The fundamental absorption edge can be seen to shift slightly toward longer wavelengths. Exactly similar behavior has been observed by Fan and Ramdas[10,14] for n- and p-type silicon irradiated to high resistivities by

---

*We are indebted to Dr. H. Richtol of the RPI Chemistry Department for allowing us to use his low temperature infrared cell.

a) reactor neutrons, b) 9 Mev deuterons and c) electrons of energy less than 4.5 Mev. In Fig.11 is shown the radiation-induced 1.8 micron band measured at 295°K for an oxygen-containing p-type and a floating zone n-type silicon sample after irradiation

From Figs. 10 and 11 it can be seen that the defect responsible for the band at 1.8 microns is found in both oxygen-containing ($\sim 10^{18}$ oxygen atoms/cm$^2$), and floating-zone silicon ($10^{15}$ - $10^{16}$ oxygen atoms/cm$^3$). The relative oxygen concentration is determined by a comparison of the intensity of 9 micron oxygen band in floating zone and crucible grown silicon. In addition, the defect giving rise to 1.8 micron band is apparently independent of the chemical impurity (phosphorous in n-type, boron in p-type).

Because the irradiated samples all had high resistivity after the irradiation ($1 - 2 \times 10^{18}$ e/cm$^2$) we can use the conclusions of Fan and Ramdas[10] that one does not observe the 1.8 micron band unless the Fermi level is about 2 kT below the 0.21 ev level responsible for the defect absorption band at 1.8$\mu$. Since the Fermi level has to be in a certain

range of the forbidden gap for observation of 1.8 $\mu$ band then according to Fan and Ramdas[10] the defect center must be associated with electronic excitation rather than ionization[10].

Fan and Ramdas[11] do not observe the 1.8 $\mu$ band in floating zone silicon irradiated by 4.5 Mev electrons, and they find that oxygen dispersed through the silicon is necessary to observe the 1.8 $\mu$ band with 4.5 Mev electron irradiations. The 1.8 $\mu$ band is observed by Fan[10,11] in 9.6 Mev deuteron and neutron irradiation of both oxygen-free and floating-zone silicon and they conclude that the defect center of the 1.8 $\mu$ band consists of a "combination" or cluster of simple vacancies and interstitials which results from energetic primary knock-ons from 9.6 Mev deuterons and fast neutrons $E \gtrsim 0.1$ Mev from the reactor spectrum. According to Fan it appears the defect center of the 1.8 micron band is formed more efficiently by 4.5 Mev electron irradiation if oxygen is present in the sample. Fan[11] has shown further that for the case of 9.6 Mev deuteron bombardment the 1.8 micron band is produced at 1/2 the rate in floating zone compared to oxygen-containing silicon. Examination of our results in Figs. 10 and 11 taking into consideration the different sample thicknesses shows that the 1.8 $\mu$ band is produced about four times more efficiently in oxygen-containing silicon than in floating-zone, in agreement with Fan's results.

From a study of the dichroic effect of pressure on the 1.8$\mu$ band Fan and Ramdas[11] suggest that the simplest model for this defect is that of two vacancies or two interstituals on the next nearest sites. The role of oxygen in this defect center is not known. A precise study of the configuration of the defect can perhaps only be gotten definitively from spin resonance studies.

Proceeding on to the longer wavelength region the next radiation-induced defect absorption bands observed were in the 3-4$\mu$ range. Figure 12 shows the infrared spectra of the pulled and floating zone n-type silicon measured in the 3 to 4$\mu$ range at 295$^{o}$K and 85$^{o}$K. In both cases sharp bands appear at 3.46 and 3.62$\mu$ when the sample is cooled to $\sim$ 85$^{o}$K with the effect appearing more pronounced in the floating-zone sample. In the thicker floating-zone sample there appears an indication of broad absorption from 3.1 to about 3.7$\mu$, while for the pulled crystal broad absorption is not present. Similar infrared spectra for another floating-zone n-type and a crucible-grown p-type silicon sample are shown in Fig. 13. Here again we observe the 3.46 and 3.62$\mu$ bands in both samples only at 85$^{o}$K, and the thicker floating-zone sample shows a slight indication of broad absorption from 3.1 to about 3.7$\mu$. The samples have the thicknesses given given in Figs.10 and 11 and in Table I. The bands shown in Figs.12 and 13 have also been

observed by Fan and Ramdas[10] in neutron-irradiated and electron-irradiated ($E \lesssim 4.5$ Mev) n-type silicon (See Fig. 3 of Reference 10). Very nearly the same temperature dependence as we find in Figs. 12 and 13 was observed by Fan and Ramdas in that the bands become sharp and pronounced at $\approx 90^{\circ}K$ and broadened into a less intense band at $300^{\circ}K$ and $383^{\circ}K$. However, they[10] did not find these bands in p-type or high resitivity n-type silicon, and concluded the absorption center has a defect energy level 0.21 ev below the conduction band. It has been suggested[10] that these bands arise from centers slightly different from each other in energy as excited states near the ground state.

Since the results given in Figs. 10-13 are very similar to those found for neutron and 4.5 Mev electron irradiated pulled silicon it appears to be a reasonable conclusion that the bands are all caused by the same type defect centers in different states of ionization lending further credance to Fan and Ramdas conclusion[10].

The next known radiation-induced defect absorption (prior to heat treatment) band has been found in neutron irradiated n-type silicon by Fan and Ramdas[10], and in 22 Mev proton irradiated silicon by G. Hill[16] at 5.5 $\mu$. This band was not observed in any of our silicon samples irradiated with 40 Mev electrons. The results of Fan[10] and Hill[16] show that the 5.5 $\mu$ absorption is very weak $\lesssim$ 5% transmission change. We shall comment further on the 5.5 $\mu$ band in a later part of the text.

The longest wavelength defect absorption bands which we observed were in the 10 to 12 micron region. These bands were only observed in the oxygen-containing silicon samples. In order to observe the very sharp radiation-induced bands in this wavelength range the wavelength span was increased by a factor 10 and the spectrometer was run very slowly. It was necessary to perform these measurements carefully otherwise the bands would not have been observed; in fact, previous work of Corbett[12] using 1.4 Mev electrons and Ramdas and Fan[13] using neutrons and 4.5 Mev electrons on pulled silicon was used as a guide in our work. In Fig.14 is shown the 12 micron (835 $cm^{-1}$) band for the pulled n-type silicon irradiated with 36 Mev electrons to 2.2 X $10^{18}$ $e/cm^2$. Although not shown in Fig.14 extremely sharp yet weaker bands at 10.1 and 11.6 microns were observed for this sample. Defect absorption bands at 10.1, 11.6 and 12 microns were also observed for the pulled p-type silicon sample irradiated with 44 Mev electrons to 1.7 X $10^{18}$ $e/cm^2$. However, the bands were all relatively weaker than for the n-type silicon shown in Fig. 14.

From Fig. 14 it can be seen that the absorption band at 12 $\mu$ shifts to shorter wavelength as the temperature is decreased from room temperature down to about 85°K. It has been shown by spin resonance[17] and infrared[12] measurements that the defect responsible for the absorption band at 12 microns

(835 $cm^{-1}$) is an oxygen vibrational band composed of a substitutional oxygen atom coupled to a vacancy. This defect has been called the "Si-A" center and the energy state of this defect gives rise to an energy level 0.17 ev below the bottom of the conduction band. We have observed this energy level from temperature dependence of carrier concentration of 40 Mev electron-irradiated silicon and was given in a previous report. This same state at $E_c$ - 0.17 ev has been observed from electrical properties in 1 Mev[18] and 4.5 Mev[19] electron-irradiated silicon.

Since we are not able to observe the 12 micron band in oxygen-free silicon we conclude that the defect responsible for the absorption in Fig.14 is indeed the "Si-A" center of Watkins. Moreover the temperature dependence of the 12$\mu$ band is exactly the same as that observed by Corbett et al.[12], and in fact our Fig.14 appears exactly like the absorption spectrum given in Fig.13 of Corbett's paper[12].

We shall conclude by a discussion of the defect bands at 5.5$\mu$ and 20.5$\mu$ which have been formed by Fan and Ramdas by neutron irradiation. The 20.5$\mu$ band has also been observed by Balkanski et al.[15] silicon irradiated by reactor neutrons. In both cases the 20.5$\mu$band is present with intensity nearly equal to the normal silicon lattice

band at 16.5$\mu$ and therefore is easy to detect. If one reasons that since our electron energy $\sim$ 40 Mev can only impart a maximum of $\sim$ 14 Kev to the silicon atom while neutrons of $\sim$ 1.0 Mev impart similar maximum recoil energy it is probably true that the 20.5$\mu$ band is only induced by radiation giving more than $\sim$ 14 kev to the silicon atom. It is realized that the fission spectrum contains a large number of neutrons having energies greater than 1 Mev. Therefore it is concluded from the fact that we did not observe a band at 20.5$\mu$ that the defect responsible must be a complex aggregate or cluster of vacancies, interstitials and impurities. In order to check this possibility we shall perform an electron irradiation using $\sim$ 60 Mev electrons which impart the same maximum recoil energy to silicon as $\sim$2 Mev neutron. High flux 60-Mev electrons can be achieved in the RPI linac.

Annealing Experiments

In the coming six month period we shall measure the infrared spectra of all samples after about 30 minute anneals at temperatures from 150°C to 500°C in 25°C steps. The annealing experiments will help support the finding that we do in fact observe the "Si-A" center if annealing characteristics similar to the Corbett[12] results are found. This work will constitute the B.Sc. thesis to be written by Mr. Gordon Oehler of the Electrical Engineering Department at Rensselaer Polytechnic Institute.

# 12-52 MEV ELECTRON IRRADIATION OF SILICON AND GERMANIUM AT $\sim 300^{\circ}K$

In continuing our studies of defect energy levels in the forbidden gap, and energy dependence of defects introduced by 12 to 52 Mev electrons (at $300^{\circ}K$ irradiation) in silicon and germanium the following bombardments were completed recently. The samples irradiated in this experiment were:

1) Floating-zone p-type silicon (Boron doped) 10 $\Omega$-cm (nominal)
2) p-type germanium (Indium-doped) 1 $\Omega$-cm (nominal)
3) n-type germanium (Arsenic-doped) 10 $\Omega$-cm (nominal)
4) n-type germanium (Antimony-doped) 10 $\Omega$-cm (nominal)

The samples were bombarded with 12, 24, 40 and 52 Mev electrons. In all cases the electrons were incident upon the sample in the <111> direction.

Conductivity Measurements

Percent changes in conductivity are given in Table II. The percent changes in conductivity for Si and P-type Ge correspond to a change in flux of $4 \times 10^{14}$ electrons/cm$^2$. The percent changes in conductivity for N-type Ge correspond to a change in flux of $4 \times 10^{12}$ electrons/cm$^2$. The percent change in conductivity decreased (in general) with an increase in energy. Figures 15,16,17 and 18 show the conductivity plotted as a function of integrated flux. In all cases the conductivity decreases with an increase in flux.

Hall Coefficient Measurements

TableIII gives the percent changes in Hall Coefficient. The flux changes used for these calculations were the same as those used for percent change in conductivity. The percent change in Hall coefficient decrease (in general) with an increase in energy. All cases show an increase in the Hall coefficient with an increase in flux. Hall coefficients as a function of flux are shown in Figures16,17 and 19. Hall coefficient of p-type silicon was not measurable due to low magnetic flux attainable with the power supply available. In all samples the Hall mobility change during irradiation was less than a 10-15% decrease, and we have not presented Hall mobility vs integrated flux in our results.

Carrier Concentration and Carrier Removal Rates

Figures 20,21 and 22show the carrier concentration of n-and p-type germanium as a function of flux. Figure 23shows the carrier removal rates as a function of energy. For N-type Ge the shape of the carrier removal rate curves vs energy is in good agreement with the theoretical curve. P-type Ge shows a decrease in the rate of removal of carrier with an increase in energy; this result is somewhat surprising and needs further investigations. In Table IV are given the measured carrier removal rates (at $300^{o}K$) and a comparison to calculated defect introduction rates using Mott-McKinley-Feshbach scattering and

the Kinchin-Pease model. A 15 and 30 ev threshold energy was used.

At low energies it is possible that part of the electron beam is intercepted by the magnet as a result the number of electrons reaching the Faraday cup is less than the number of electrons at the sample position. Thus the flux calculated is too small. As a consequence the percentage change in conductivity and Hall coefficient is perhaps too large at 12 Mev. This question will be checked in great detail during the next irradiation series.

During the next 6 month period temperature cycling runs on the carrier concentration and conductivity will be made to ascertain the position of each defect energy level responsible for trapping carriers.

# CARRIER LIFETIME STUDIES IN ELECTRON (10-55 Mev) AND PROTON - (25-110 Mev) IRRADIATED GERMANIUM

by
John E. Fischer and John C. Corelli

A paper covering the above mentioned research will be submitted for publication in the Journal of Applied Physics. Preprint copies will be sent separately to NASA Headquarters, Washington, D.C., and NASA Langley Research Center, IRD-Bldg. 1230, Hampton, Virginia. In this progress report we have included the abstract and a summary of the paper as it will appear in its finished form.

## ABSTRACT

Samples of single-crystal germanium were irradiated at room temperature with electrons of energies from 12 Mev to 55 Mev and with protons of energies from 25 Mev to 109 Mev. Measurements of the minority carrier lifetime as a function of flux and initial carrier concentration suggest that:

1) More than one recombination level is introduced into the forbidden gap by the defects created during electron and proton bombardment, with the multilevel effect being greater for the proton-irradiated specimens.

2) Nonlinearity of the defect introduction rates of two proton-irradiated samples may be due to the closing of channels[20,21] and the resulting decrease in the number and range of "stenons" (channeled knockons).

3) The carrier lifetime change with increasing proton energy does not decrease as sharply as predicted by Rutherford scattering and the Kinchin-Pease model. This indicates that nuclear elastic and inelastic processes must be included in computing the number of primary knockons created by protons of energies above 40 Mev. The importance of channeling cannot be assessed quantitatively without better knowledge of the nuclear cross-sections.

4) The energy dependence of carrier lifetime change in the case of electron bombardment is complicated by a non-constant contribution of multiple levels to the recombination process in the electron energy range studied. At 12 Mev the behavior is adequately represented by single-level theory and a value of 15.4 displacements/cm. is obtained, which is derived using a displacement threshold of 15 ev.

## SUMMARY

The experimental results presented herein suggest the following: a) Detailed information concerning the damage process, namely the enhancement of damage by the closing of channels and the attendant reduction in the number and range of stenons, may be obtained from anomalies in the flux dependence of $1/\tau$ if surface effects and Fermi level changes can be ruled out or accounted for. One would expect the percent increase in slope of $1/\tau$ vs. flux to be greater for higher bombarding energies since more of the total knockon energy would have been dissipated in glancing stenon collisions before the channels were closed. b) The clustering of defects into aggregates at high bombarding energy produces two classes of energy levels. The most predominant type, which are probably associated with defects of atomic dimensions, determine the lifetime in germanium irradiated with 1 and 12 Mev electrons. The presence of the second, or cluster-associated class, becomes evident at 23 Mev and increases through 39 and 54 Mev. In the case of proton bombardments the degree of deviation from single-level behavior is independent of energy from 25 to 85 Mev and is larger than that observed in the electron irradiations. The fact that measurements of the temperature dependence of carrier concentration[20] exhibit more than one level suggests that cluster associated defects act as recombination centers and as permanent

carrier traps; however the efficiency of cluster defects as recombination centers is higher than for carrier traps. c) Comparison of experiment with theoretical predictions of the energy dependence of defect introduction rate by electrons from 12 to 55 Mev is complicated by the fact that the degree of clustering is not constant in this energy range. The defect introduction rate at 12 Mev is 15.4 displacements/cm $\pm$ 20% and agrees with theory, although the effect of channeling cannot be estimated due to the large flux error. Calculations show that a channeling probability P as small as 0.10 which is not unreasonable for germanium, reduces the displacement cross-section by 20% for a 20 Mev electron, by 50% for a 100 Mev electron. d) The energy dependence of the relative defect introduction rate by protons from 25-110 Mev clearly shows the necessity of including nuclear elastic and inelastic processes in the calculations of defect introduction rates. The importance of channeling is suggested by anomalies in $1/\tau$ vs. flux, but its quantitative effect on the defect introduction rate must await evaluation until the primary cross sections for germanium are known more accurately.

# PROTON IRRADIATION OF GERMANIUM AT $\sim 300^{\circ}K$ BY 25 AND 110 MEV PROTONS

In order to check the occurrance of shallow acceptor states induced by protons in n-type Ge, $\lesssim$ 0.1 ev below the bottom of the conduction band, an experiment was performed using the proton beam (E=150 Mev) of the Harvard University* cyclotron. In our previous progress report we had concluded from only meager evidence that a shallow acceptor level at $\sim$ 0.08 ev was found in n-type germanium irradiated with 20 Mev protons. It was pointed out to us by Dr. John W. MacKay+ that our data did not show in a definitive manner the existence of this shallow level, and hence we made , during the past 6 month period, a careful investigation of this point. We shall only give a brief summary of our findings in this report.

Bridge samples 20-28 mils thick were used which were suitable for Hall effect and conductivity measurements. During bombardment at Harvard only the conductivity was monitored. A summary of the bombardment data is given in Fig. 24 where the quantity $\frac{\sigma_0 - \sigma}{\sigma_0}$ is plotted as a function of proton energy, $\sigma_0$ and $\sigma$ are the conductivity before and after an

---

* The assistance of Mr. Andy Koehler, Assistant Director of the Harvard University Cyclotron, is gratefully acknowledged

+ Dr. John W. MacKay, private communication

integrated proton flux of $2 \times 10^{11}$ p/cm$^2$. The arsenic-doped germanium appears to be damaged slightly less than the antimony-doped germanium. The results of Fig.24 indicate that the energy dependence of damage does not follow simple Rutherford scattering. A similar conclusion was reached by us in using the carrier lifetime to detect defects. Theoretical analysis of the energy dependence of proton-induced damage in germanium is currently being analyzed by Mr. E. Saunders and Dr. G. P. Calame. Their results will become available upon completion.

In Fig.25 we show the temperature dependence of the Hall coefficient for two antimony-doped germanium samples irradiated by 25 Mev proton to integrated fluxes shown on the figure. Only a shallow acceptor level at $\sim$ 0.24 ev and a deeper level are in evidence in agreement with our previous work. There is <u>no indication</u> of a shallow level at $\sim$ 0.1 ev below the bottom of the conduction band in agreement with Dr. MacKay's results. This conclusion was the basis for performing the experiment. Future work in proton bombardments will be continued in close collaboration with NASA Langley Research Center IRD personnel.

TABLE I

| Sample No. | Type and Impurity | Initial* Resistivity | Crystal Growing Method | Incident Energy | Total Integrated Flux | Thickness mm |
|---|---|---|---|---|---|---|
| 1 | n-Type Phosphorous | 0.09 Ω-cm | Floating Zone | 40 Mev | $1.5X10^{18}e/cm^2$ | 7.37 |
| 2 | n-Type Phosphorous | 0.1 Ω-cm | Floating Zone | 44 Mev | $1.7X10^{18}e/cm^2$ | 9.00 |
| 3 | p-Type Boron | 200 Ω-cm | Pulled from Crucible | 44 Mev | $1.7X10^{18}e/cm^2$ | 2.45 |
| 4 | n-Type Phosphorous | 80 Ω-cm | Pulled from Crucible | 36 Mev | $2.2X10^{18}e/cm^2$ | 2.41 |

*Pre-irradiation values at 300°K.

TABLE II

Percent Change in Conductivity

| Sample | Electron Energy (MEV) | Type | % Change | Resistivity ohm-cm |
|---|---|---|---|---|
| Si (B) | 12 | P | 15.3 | 10.3 |
| | 24 | P | 12.6 | 5.23 |
| | 40 | P | 12.7 | 9.08 |
| | 52 | P | 10.0 | 18.8 |
| Ge (In) | 12 | P | 22.1 | 1.02 |
| | 24 | P | 19.8 | .87 |
| | 40 | P | 13.4 | .92 |
| | 52 | P | 10.9 | .94 |
| Ge (As) | 24 | N | 18.6 | 9.11 |
| | 40 | N | 8.84 | 14.1 |
| | 52 | N | 14.9 | 8.42 |
| Ge (Sb) | 12 | N | 27.3 | 11.3 |
| | 24 | N | 16.6 | 16.6 |
| | 40 | N | 11.4 | 13.7 |

TABLE III

Percent Change in Hall Coefficient

| Sample | Electron Energy (MEV) | Type | % Change | Resistivity ohm-cm |
|---|---|---|---|---|
| Ge (In) | 12 | P | 25.6 | 1.02 |
| | 24 | P | 24.1 | .89 |
| | 40 | P | 14.0 | .92 |
| | 52 | P | 10.9 | .94 |
| Ge (As) | 24 | N | 19.6 | 9.11 |
| | 40 | N | 13.9 | 14.1 |
| | 52 | N | 13.5 | 8.42 |
| Ge (Sb) | 12 | N | 34.5 | 11.3 |
| | 24 | N | 57.9 | 16.6 |
| | 40 | N | 16.3 | 13.7 |

TABLE IV

Carrier Removal Rates

| Sample | Evergy (Mev) | Resistivity ohm-cm | Ed=15ev | Ed=30ev | Measured |
|---|---|---|---|---|---|
| Ge (In) | 12 | 1.02 | 16.8 | 9.2 | 1.25 |
| P-Type | 24 | .89 | 20.7 | 9.3 | 1.25 |
| | 40 | .92 | 23.6 | 10.8 | 1.00 |
| | 52 | .94 | 25.0 | 11.4 | .75 |
| Ge (As) | 24 | 9.11 | 20.7 | 9.3 | 2.85 |
| N-Type | 40 | 14.08 | 23.6 | 10.8 | 5.00 |
| | 52 | 8.42 | 25.0 | 11.4 | 5.00 |
| Ge (Sb) | 12 | 11.33 | 16.8 | 9.2 | 2.05 |
| N-Type | 24 | 16.57 | 20.7 | 9.3 | 2.95 |
| | 40 | 13.65 | 23.6 | 10.8 | 3.65 |

## LIST OF REFERENCES


1. J. W. MacKay and E. Klontz, J. Appl. Phys. 30, 1269 (1959) E. E. Klontz and J. W. MacKay, J. Phys. Soc. Japan 18, Supplement III 216 (1963)
2. N. A. Kitovski, T. V. Mashovets, and S. M. Ryvkin, Soviet Physics - Solid State 4, #10 2088 (April 1963)
3. W. L. Brown, W. M. Augustyniak and T. R. Waite, J. Appl Phys. 30, 1258 (1959)
4. W. L. Brown and W. M. Augustyniak, J. Appl. Phys. 30, 1300 (1949)
5. Corelli, Cheng, Golibersuch, Merrill and Taylor, Bull. Am. Phys. Soc. Ser. II, 9, 48 (1964)
6. J. H. Crawford and J. W. Cleland, J. Appl. Phys. 30, 1204 (1959)
7. H. Y. Fan and K. Lark-Horovitz "The Effects of Radiation on Materials" Edited by J. J. Harwood et al., Reinhold p.159 (1958)
8. R. Breckenridge and C. Gross, private communication, NASA Langley Research Center, Hampton, Verginia
9. Dr. John MacKay, private communication
10. H. Y. Fan and A. K. Ramdas, J. Appl. Phys. 30, 1127 (1959)
11. H. Y. Fan and A. K. Ramdas, Proc. of the Int'l. Conf. on Semiconductor Physics, Prague (1960) p.309

12. J. W. Corbett, G. D. Watkins, R. M. Chrenko, and R. S. McDonald Phys. Rev., 121 1001, (1961)

13. A. K. Ramdas and H. Y. Fan, Jour. Phys. Soc. Japan 18, Supp. II, 33, (1963)

14. W. G. Spitzer and H. Y. Fan, Phys. Rev. 109, 1011, (1958)

15. M. Balkanski and W. Nazarewicz, Jour. Phys. Soc. Japan 18, Supp. II 37, (1963)

16. G. Hill, NASA Langley Research Center Hampton, Va. (private communication)

17. G. D. Watkins and J. W. Corbett Phys. Rev. 121, 1001 (1961)

18. G. K. Wertheim, Phys. Rev. 105, 1730 (1957); 110 1272 (1958) 111,.1500 (1958)

19. D. E. Hill, Phys. Rev. 114, 1414 (1959)

20. M. T. Robinson and O. S. Oen, Phys. Rev., 132 (2385) (1963)

21. O. S. Oen and M. T. Robinson, Appl., Phys. Letters 2, 83, (1963)

# LIST OF FIGURES

Fig. 10 Infrared spectra of $\approx$ 40 Mev electron irradiated n-type silicon (floating zone, and pulled crystal) showing the temperature dependance of the 1.8 micron defect absorption band.

Fig. 11 Infrared spectra of $\approx$ 40 Mev electron-irradiated n-type silicon (floating zone) and p-type silicon (pulled crystal) showing the 1.8 micron defect absorption band.

Fig. 12 Infrared spectra of $\approx$ 40 Mev electron irradiated n-type silicon (floating zone, and pulled crystal) showing the 3.46 and 3.62 $\mu$ bands at 85°K and their absence from the spectra at 295°K.

Fig. 13 Infrared spectra of $\approx$ 40 Mev electron-irradiated n-type silicon (floating zone) and p-type silicon (pulled crystal) showing the 3.46 and the 3.62 $\mu$ bands at 85°K and their absence from the spectra at 295°K.

Fig. 14 Infrared spectra of n-type silicon (pulled crystal) showing the temperature dependence of the Si-A center 12 micron band.

Fig. 15 Conductivity vs integrated electron flux for 10 $\Omega$-cm p-type silicon (floating-zone) irradiated with 12, 24, 40 and 52 Mev electrons at 300°K.

Fig. 16 Conductivity and Hall coefficient vs integrated electron flux for 1 $\Omega$-cm p-type germanium irradiated with 12, 24, 40 and 52 Mev electrons at 300°K.

Fig. 17 Conductivity and Hall coefficient vs integrated electron flux for 10 $\Omega$ -cm n-type germanium (arsenic doped).

Fig. 18 Conductivity vs integrated electron flux for 10 $\Omega$ -cm n-type germanium (antimony doped) irradiated with 12, 24, and 40 Mev electrons at 300°K.

Fig. 19 Hall coefficient vs integrated electron flux for 10 cm $\Omega$-cm n-type germanium (antimony doped) irradiated with 12, 24, and 40 Mev electrons at 300°K.

Fig. 20 Carrier concentration vs integrated electron flux for 1 $\Omega$ -cm p-type germanium irradiated with 12, 24, 40 and 52 Mev electrons at 300°K ($R_H = \frac{1}{pe}$ was used).

Fig. 21 Carrier concentration vs integrated electron flux for 10 $\Omega$ -cm n-type germanium (arsenic doped) irradiated with 24, 40, and 52 Mev electrons at 300°K ($R_H = \frac{1}{ne}$ was used).

Fig. 22 Carrier concentration vs integrated electron flux for 10 $\Omega$ -cm n-type germanium (antimony-doped) irradiated with 12, 24, and 40 Mev electrons at 300°K ($R_H = \frac{1}{ne}$ was used).

Fig. 23 Measured carrier removal rates vs incident electron energy for 10 $\Omega$ -cm arsenic and antimony doped germanium and for 1 $\Omega$ -cm p-type germanium.

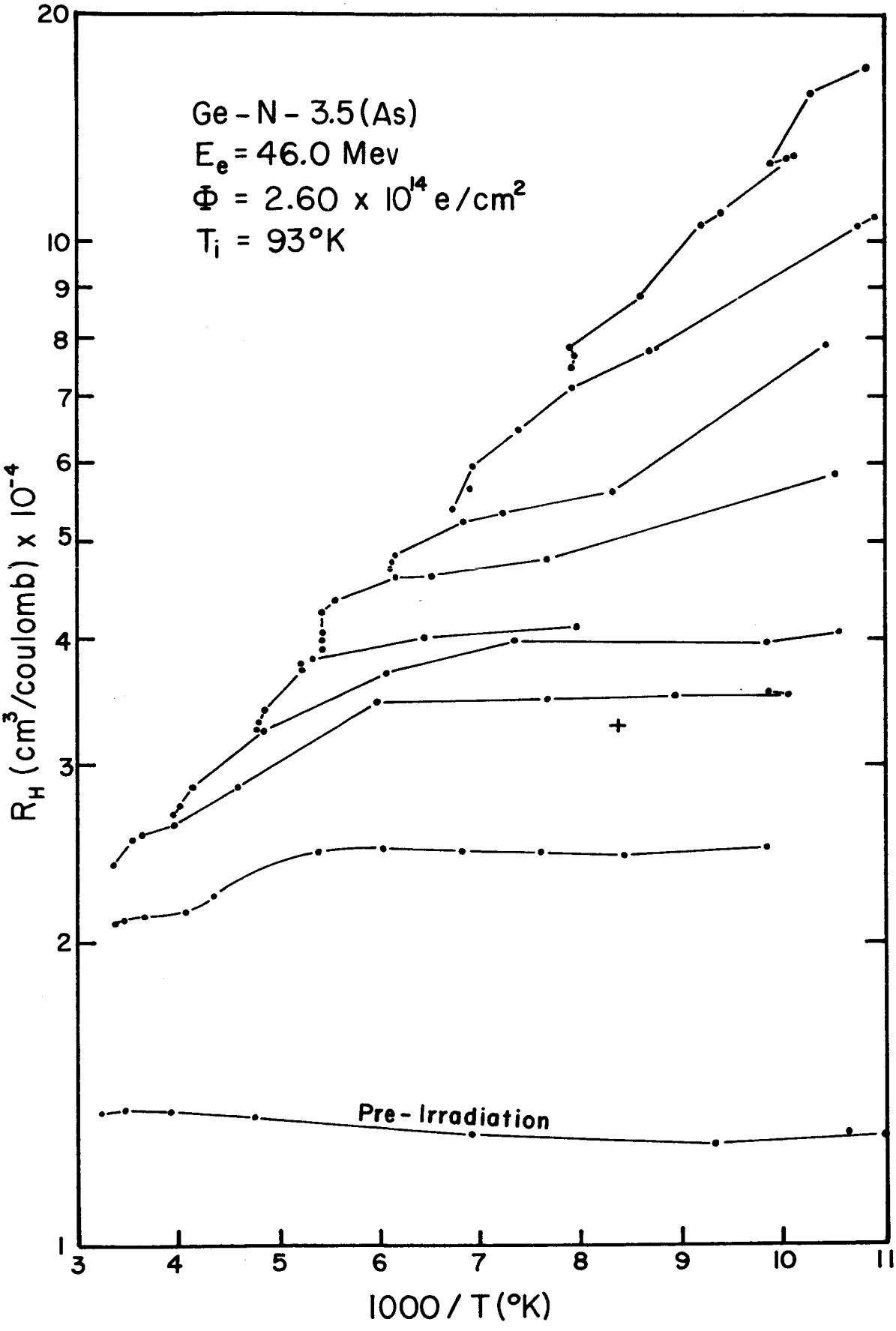
Ge - N - 3.5 (As)
$E_e$ = 46.0 Mev
$\Phi$ = 2.60 x $10^{14}$ e/cm$^2$
$T_i$ = 93°K
$R_H$ (cm$^3$/coulomb) x $10^{-4}$
1000 / T (°K)
Pre - Irradiation
20
10
9
8
7
6
5
4
3
2
1
3
4
5
6
7
8
9
10
11

Figure 1

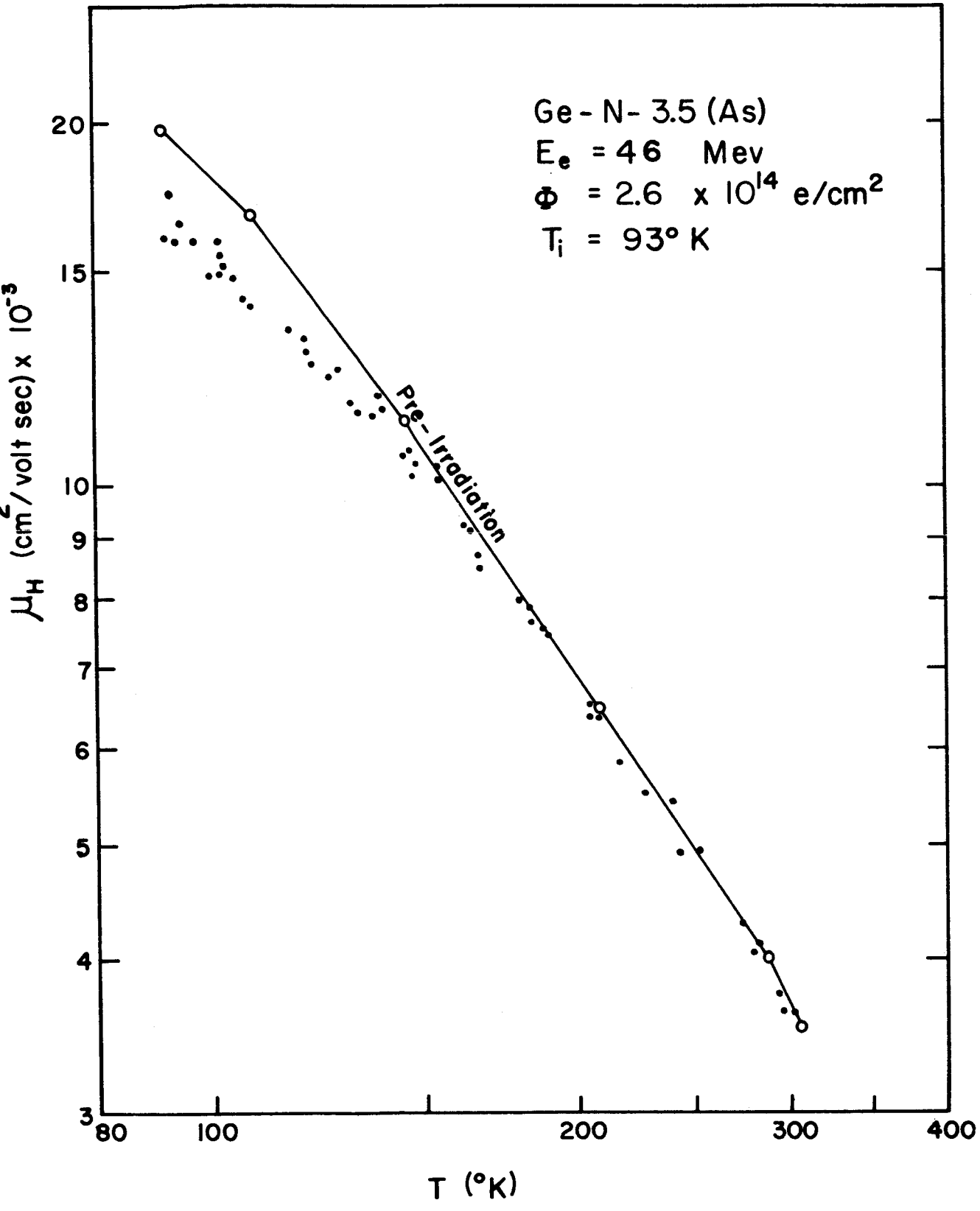
Ge - N - 3.5 (As)
$E_e$ = 46 Mev
$\Phi$ = 2.6 x $10^{14}$ e/cm$^2$
$T_i$ = 93° K
Pre-Irradiation
$\mu_H$ (cm$^2$/volt sec) x $10^{-3}$
20
15
10
9
8
7
6
5
4
3
80
100
200
300
400
T (°K)

Figure 2

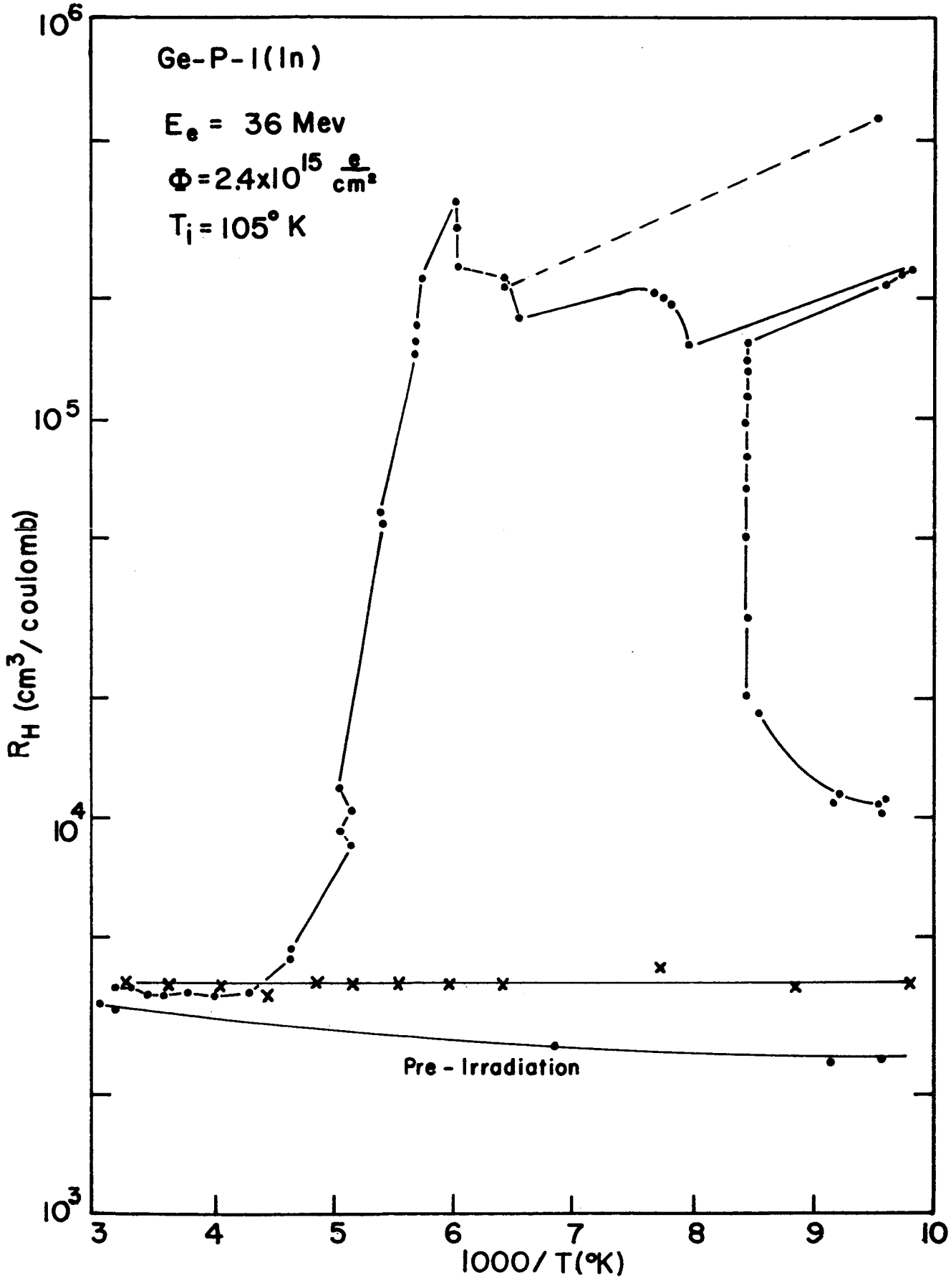
Ge-P-I(In)
$E_e$ = 36 Mev
$\Phi = 2.4 \times 10^{15} \frac{e}{cm^2}$
$T_i = 105^\circ K$
$10^6$
$10^5$
$10^4$
$10^3$
$R_H$ (cm³/coulomb)
Pre - Irradiation
3
4
5
6
7
8
9
10
1000/ T(°K)

Figure 3

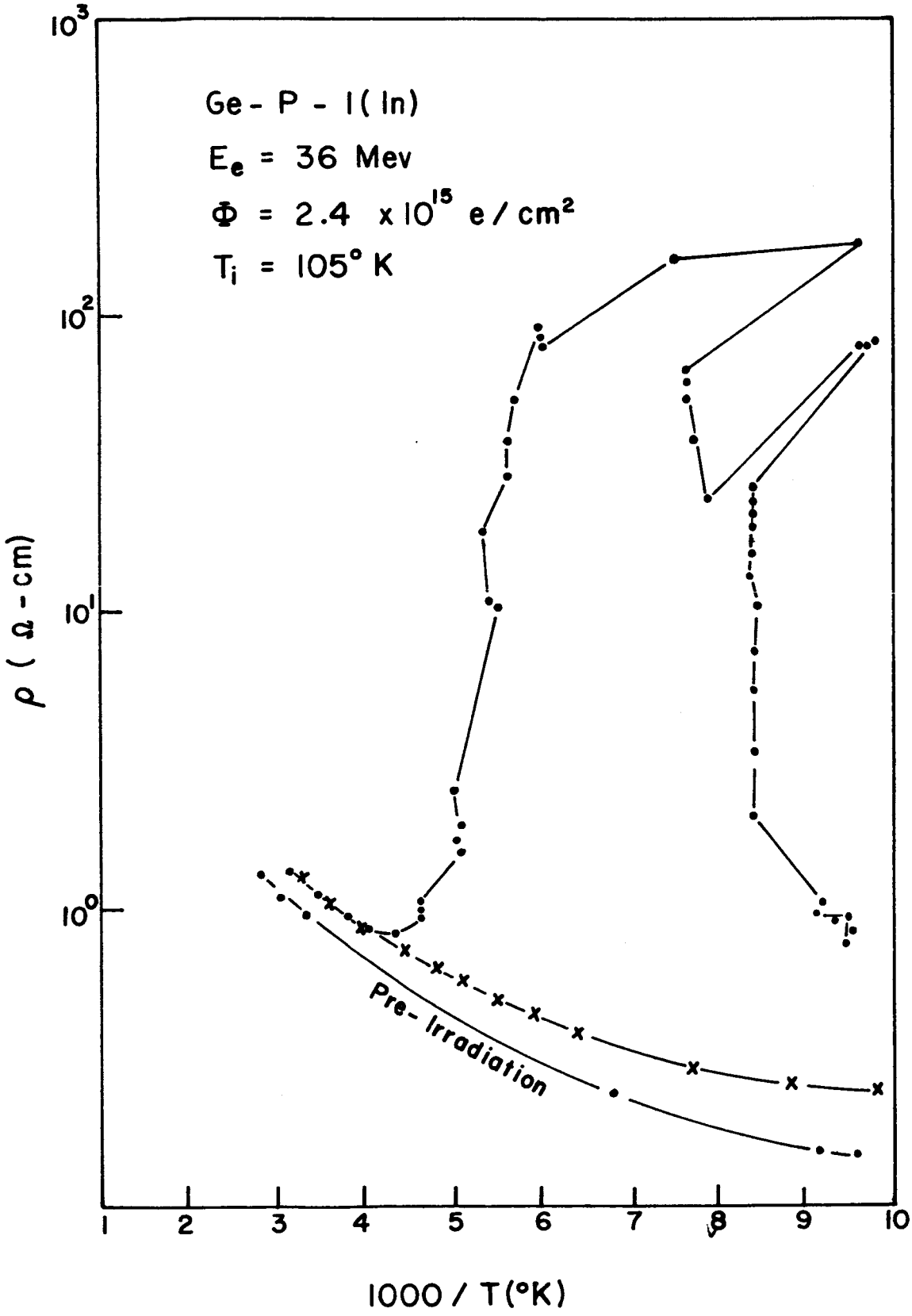
Ge - P - I ( In)
$E_e$ = 36 Mev
$\Phi$ = 2.4 x $10^{15}$ e / $cm^2$
$T_i$ = 105° K
$10^3$
$10^2$
$10^1$
$10^0$
ρ ( Ω - cm)
Pre - Irradiation
1
2
3
4
5
6
7
8
9
10
1000 / T(°K)

Figure 4

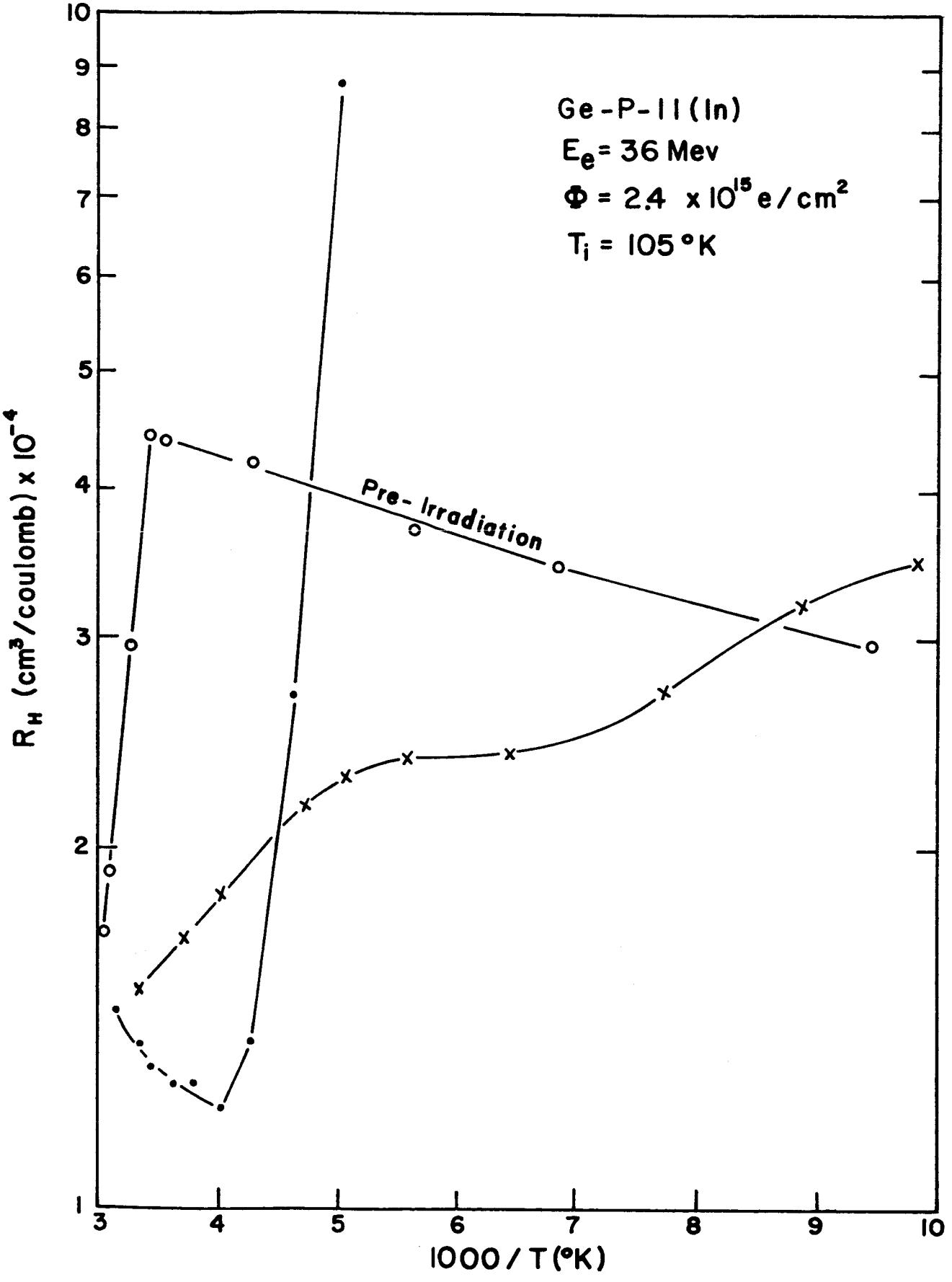
Ge-P-11 (In)
$E_e$ = 36 Mev
$\Phi$ = 2.4 x $10^{15}$ e/cm$^2$
$T_i$ = 105 °K
Pre-Irradiation
$R_H$ (cm$^3$/coulomb) x $10^{-4}$
1000 / T (°K)
10
9
8
7
6
5
4
3
2
1
3
4
5
6
7
8
9
10

Figure 5

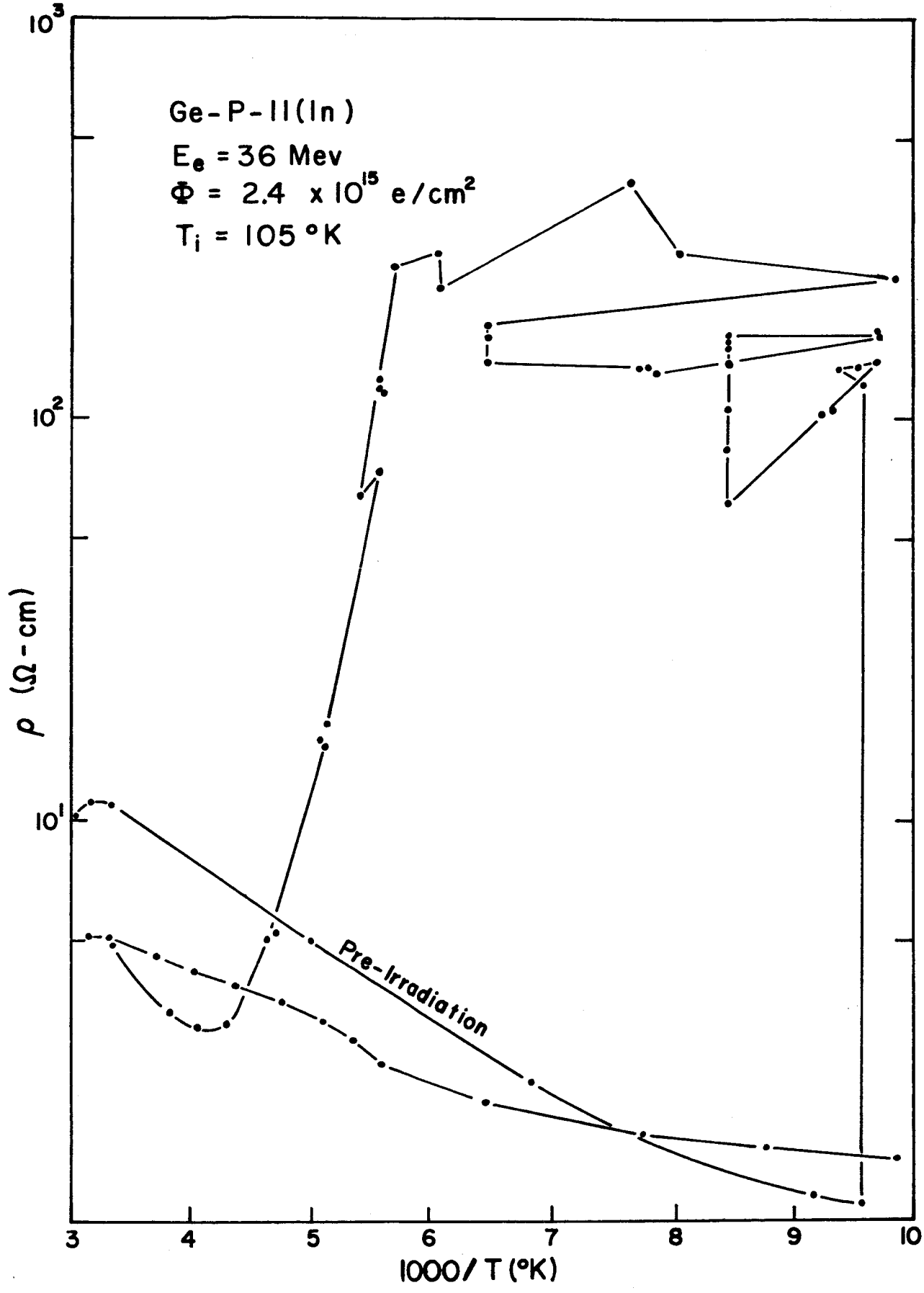
Ge-P-II(In)
$E_e$ = 36 Mev
$\Phi$ = 2.4 x $10^{15}$ e/cm$^2$
$T_i$ = 105 °K
$10^3$
$10^2$
$10^1$
ρ (Ω-cm)
Pre-Irradiation
3
4
5
6
7
8
9
10
1000/ T (°K)

Figure 6

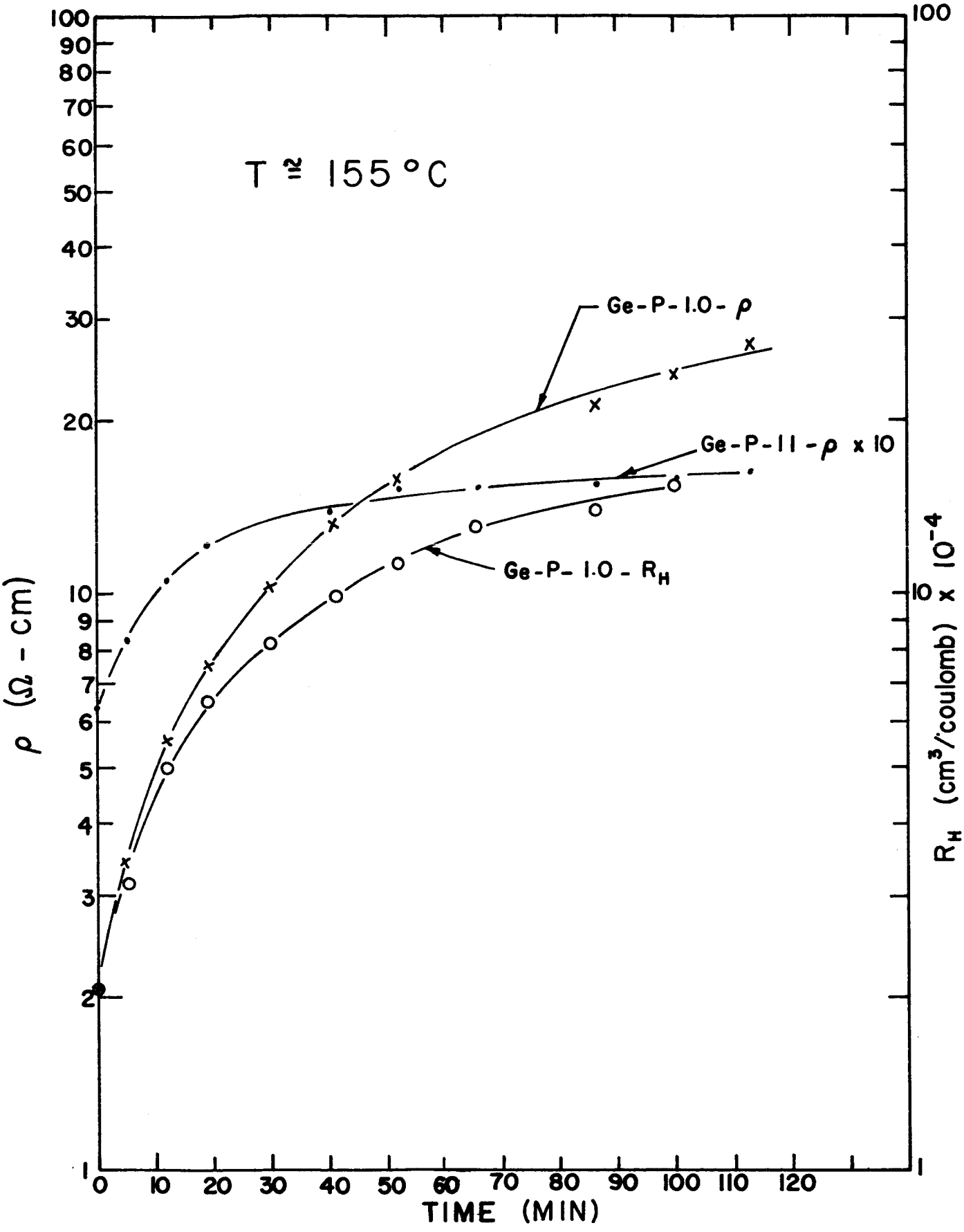
T ≅ 155 °C
Ge-P-1.0-ρ
Ge-P-11-ρ x 10
Ge-P-1.0-R_H
ρ (Ω-cm)
R_H (cm³/coulomb) x 10⁻⁴
TIME (MIN)
100
90
80
70
60
50
40
30
20
10
9
8
7
6
5
4
3
2
1
0
10
20
30
40
50
60
70
80
90
100
110
120

Figure 7

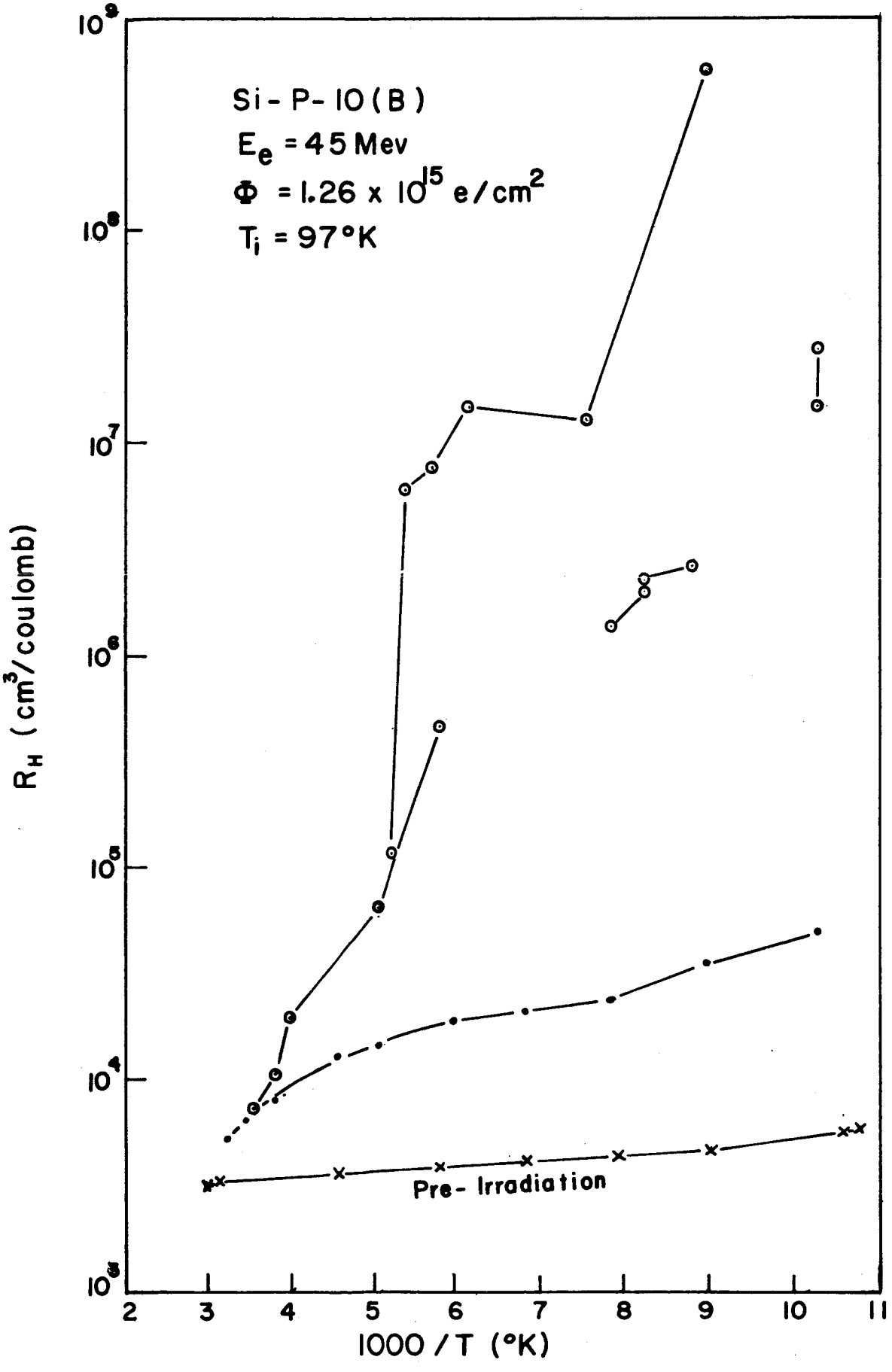
Si - P - 10 (B)
$E_e$ = 45 Mev
$\Phi$ = 1.26 x $10^{15}$ e/cm$^2$
$T_i$ = 97°K
Pre - Irradiation
$R_H$ (cm$^3$/coulomb)
1000 / T (°K)
$10^8$
$10^7$
$10^6$
$10^5$
$10^4$
2
3
4
5
6
7
8
9
10
11

Figure 8

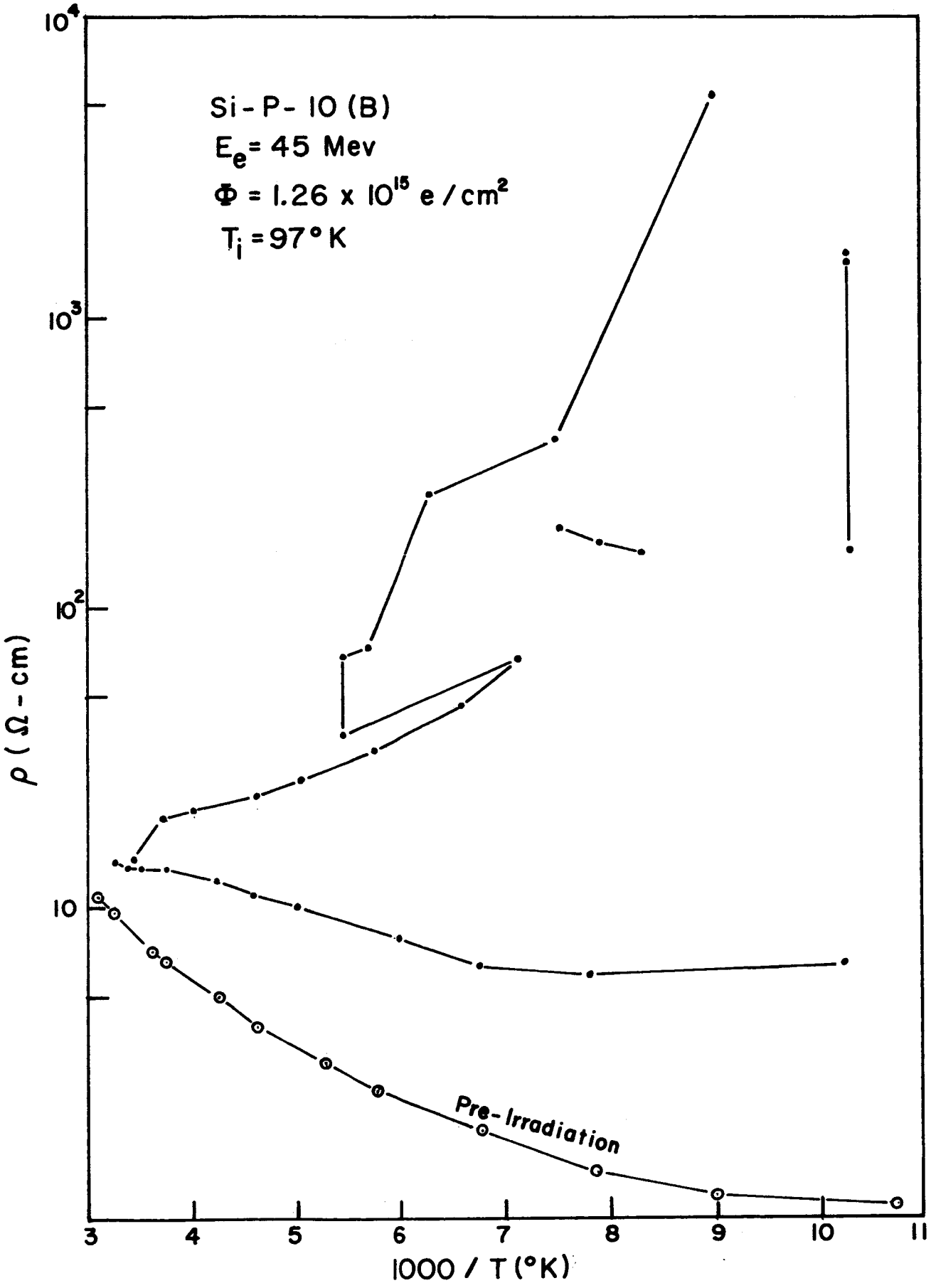
Si - P - 10 (B)
$E_e$ = 45 Mev
$\Phi = 1.26 \times 10^{15}$ e / cm$^2$
$T_i$ = 97° K
$10^4$
$10^3$
$10^2$
10
ρ (Ω - cm)
Pre - Irradiation
3
4
5
6
7
8
9
10
11
1000 / T (°K)

Figure 9

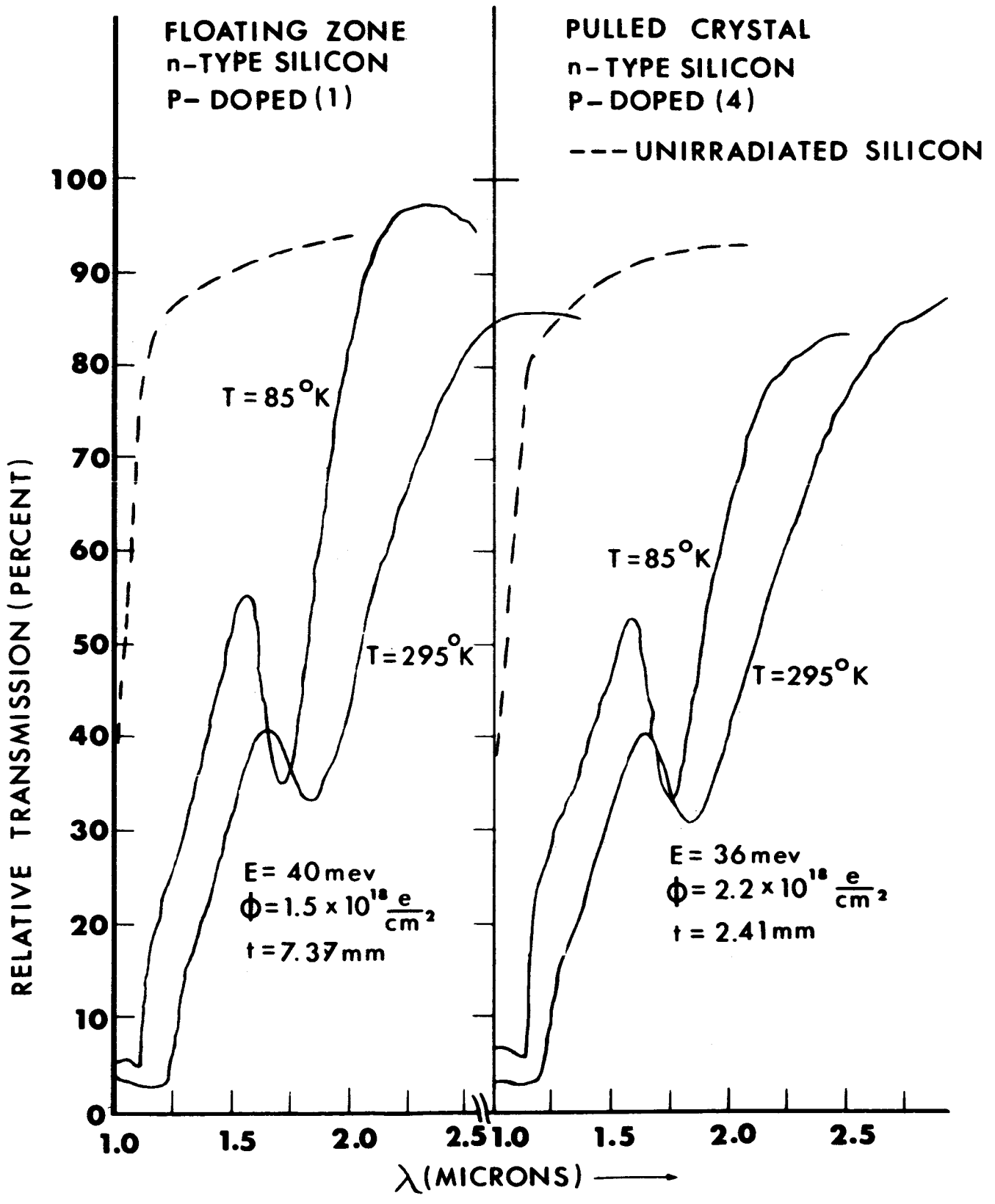
FLOATING ZONE
n-TYPE SILICON
P- DOPED (1)
PULLED CRYSTAL
n-TYPE SILICON
P-DOPED (4)
---UNIRRADIATED SILICON
RELATIVE TRANSMISSION (PERCENT)
100
90
80
70
60
50
40
30
20
10
0
T = 85°K
T = 295°K
T = 85°K
T = 295°K
E = 40 mev
Φ = 1.5 x 10^18 e/cm^2
t = 7.37 mm
E = 36 mev
Φ = 2.2 x 10^18 e/cm^2
t = 2.41 mm
1.0
1.5
2.0
2.5
1.0
1.5
2.0
2.5
λ (MICRONS) ⟶

Figure 10

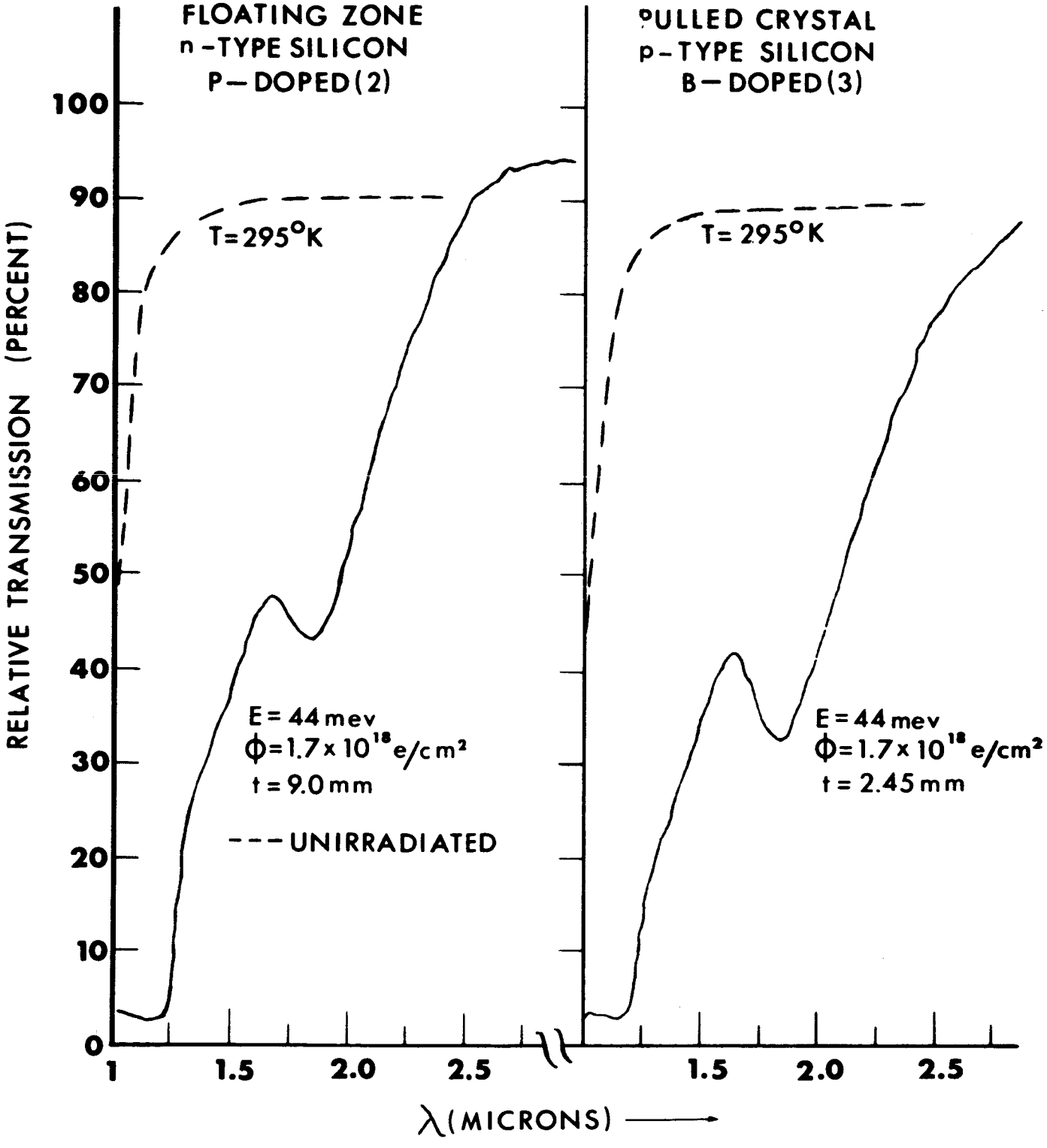
FLOATING ZONE
n-TYPE SILICON
P—DOPED(2)
PULLED CRYSTAL
p-TYPE SILICON
B—DOPED(3)
T=295°K
T=295°K
E=44 mev
Φ=1.7x10^18 e/cm²
t=9.0 mm
---UNIRRADIATED
E=44 mev
Φ=1.7x10^18 e/cm²
t=2.45 mm
RELATIVE TRANSMISSION (PERCENT)
100
90
80
70
60
50
40
30
20
10
0
1
1.5
2.0
2.5
1.5
2.0
2.5
λ(MICRONS) ⟶

Figure 11

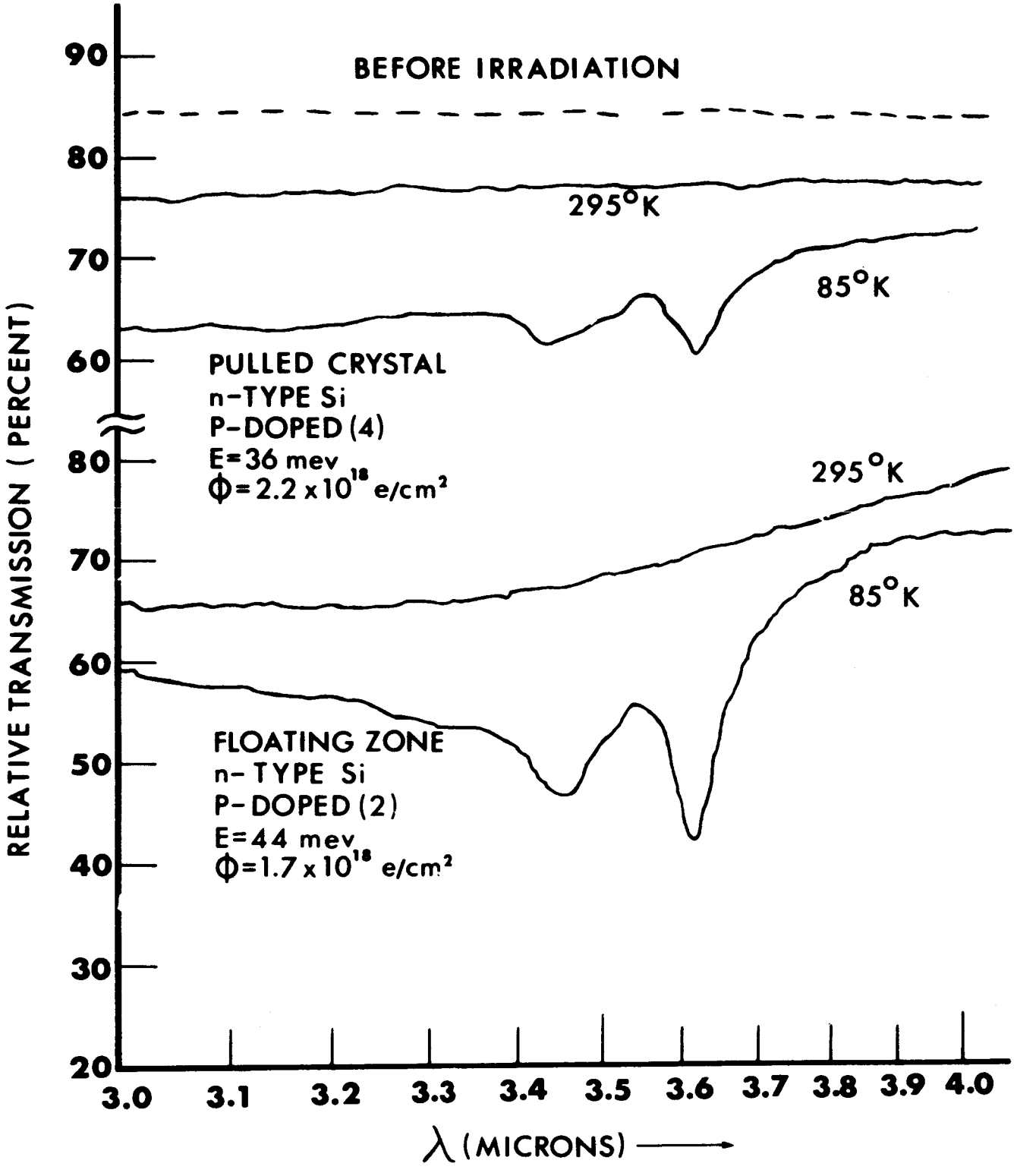
BEFORE IRRADIATION
295°K
85°K
PULLED CRYSTAL
n-TYPE Si
P-DOPED (4)
E=36 mev
Φ=2.2 x 10^18 e/cm²
295°K
85°K
FLOATING ZONE
n-TYPE Si
P-DOPED (2)
E=44 mev
Φ=1.7 x 10^18 e/cm²
RELATIVE TRANSMISSION ( PERCENT)
90
80
70
60
80
70
60
50
40
30
20
3.0
3.1
3.2
3.3
3.4
3.5
3.6
3.7
3.8
3.9
4.0
λ (MICRONS) ⟶

Figure 12

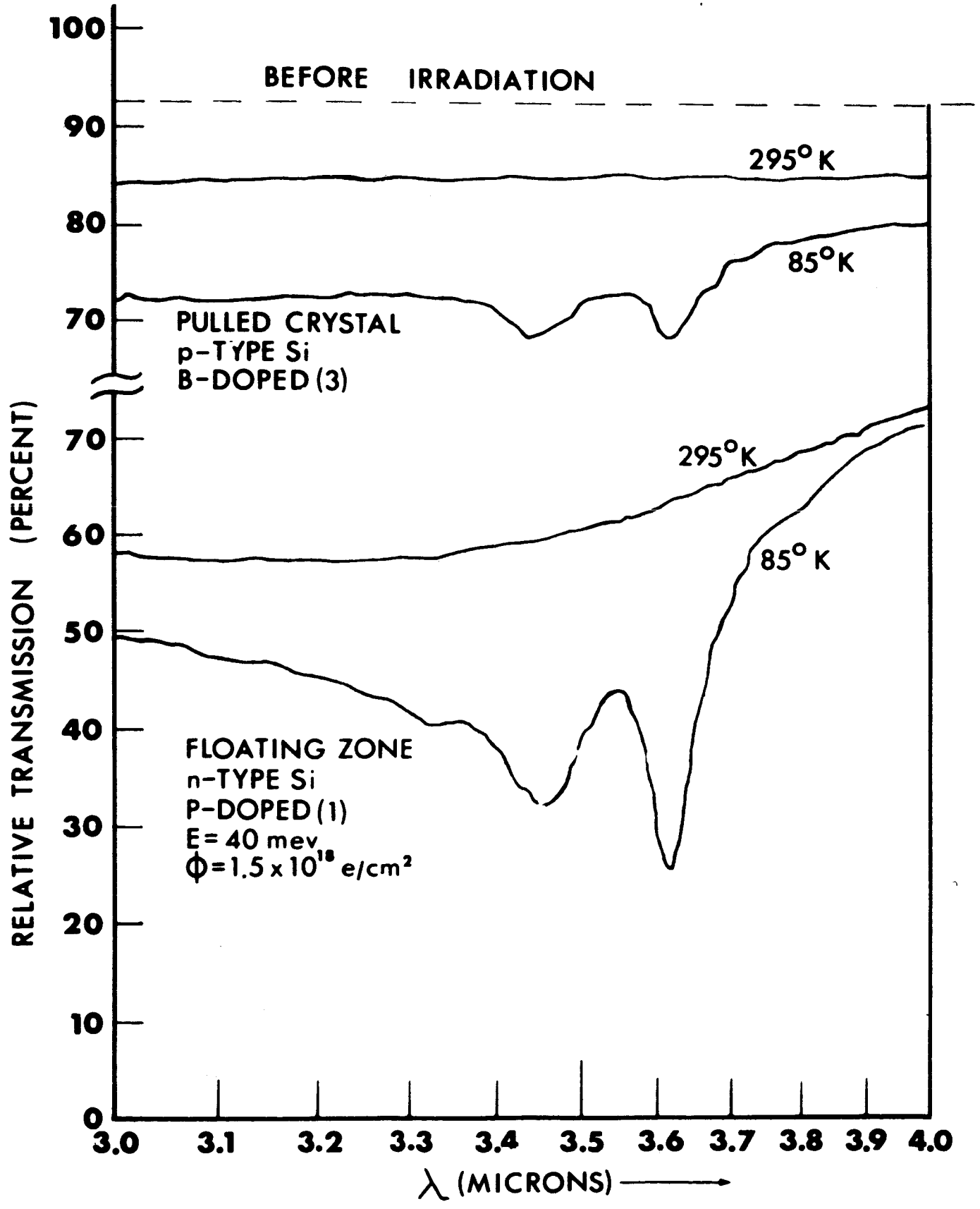
BEFORE IRRADIATION
295° K
85° K
PULLED CRYSTAL
p-TYPE Si
B-DOPED (3)
295° K
85° K
FLOATING ZONE
n-TYPE Si
P-DOPED (1)
E = 40 mev
Φ = 1.5 x 10^18 e/cm²
RELATIVE TRANSMISSION (PERCENT)
100
90
80
70
70
60
50
40
30
20
10
0
3.0
3.1
3.2
3.3
3.4
3.5
3.6
3.7
3.8
3.9
4.0
λ (MICRONS)

Figure 13

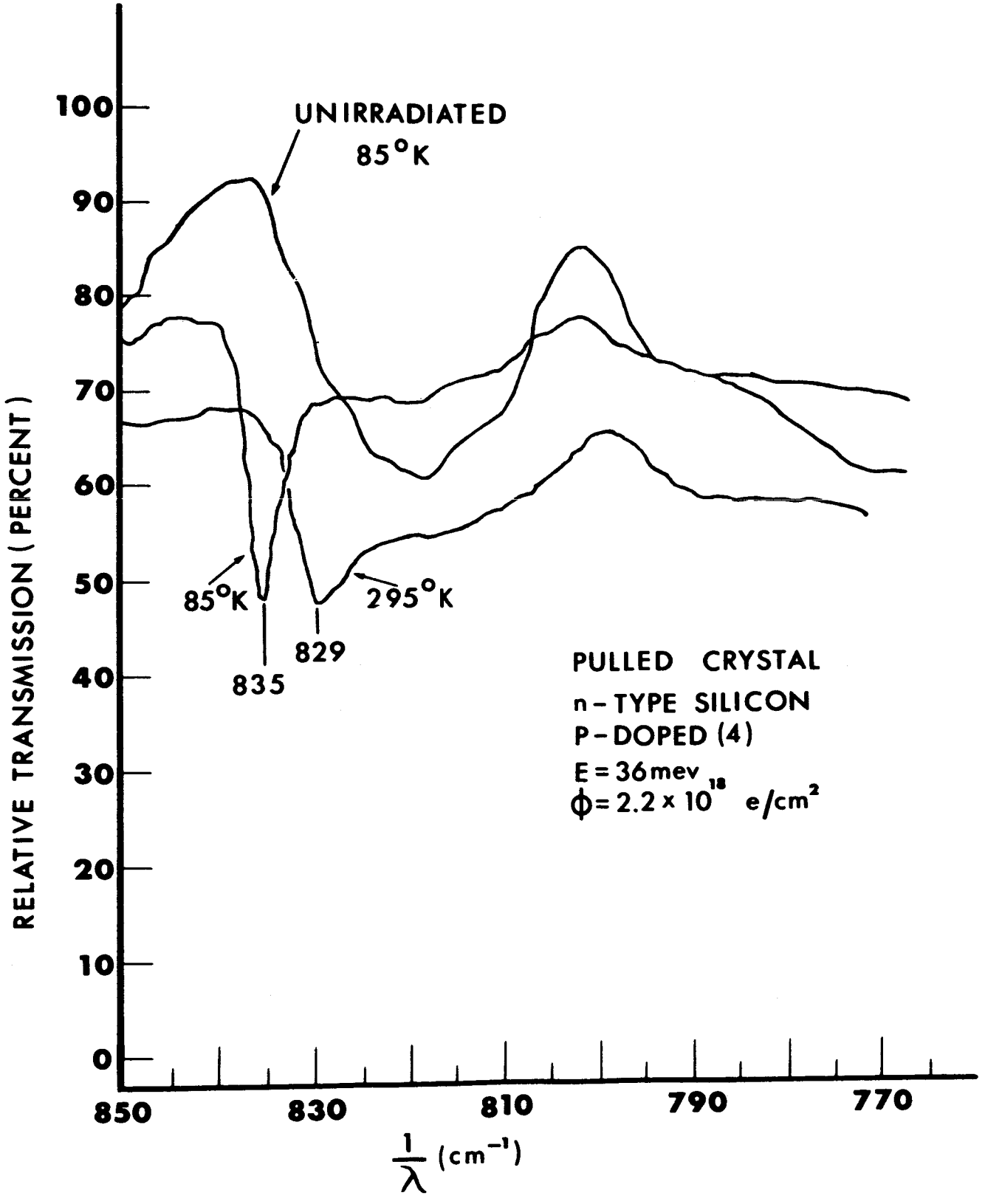
UNIRRADIATED
85°K
85°K
295°K
835
829
PULLED CRYSTAL
n-TYPE SILICON
P-DOPED (4)
E = 36mev
$\phi = 2.2 \times 10^{18}$ e/cm²
RELATIVE TRANSMISSION (PERCENT)
100
90
80
70
60
50
40
30
20
10
0
850
830
810
790
770
$\frac{1}{\lambda}$ (cm⁻¹)

Figure 14

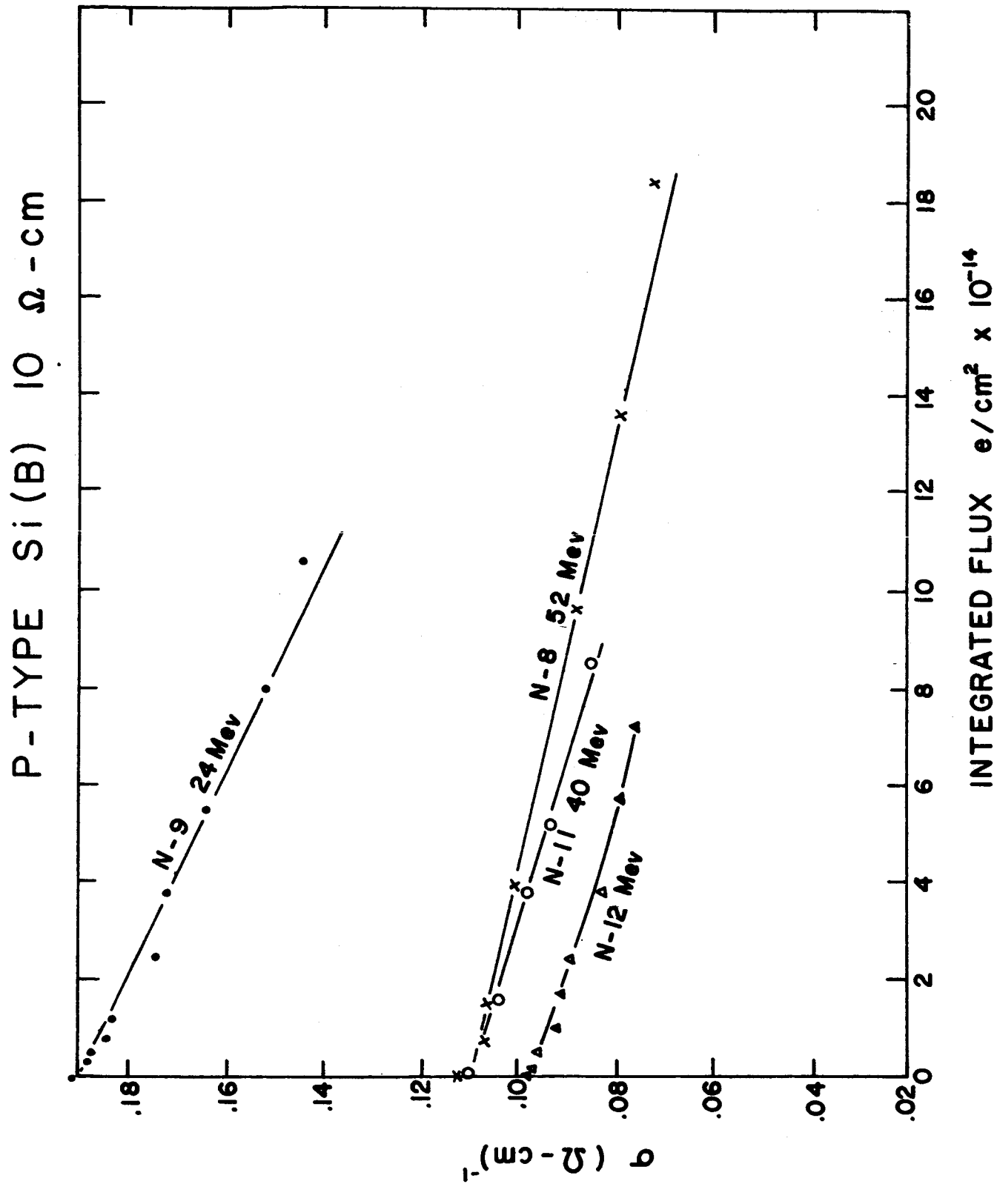
P-TYPE Si(B) 10 Ω-cm
INTEGRATED FLUX e/cm² x 10⁻¹⁴
σ (Ω-cm)⁻¹
N-9 24 Mev
N-8 52 Mev
N-11 40 Mev
N-12 Mev
.18
.16
.14
.12
.10
.08
.06
.04
.02
0
2
4
6
8
10
12
14
16
18
20

Figure 15

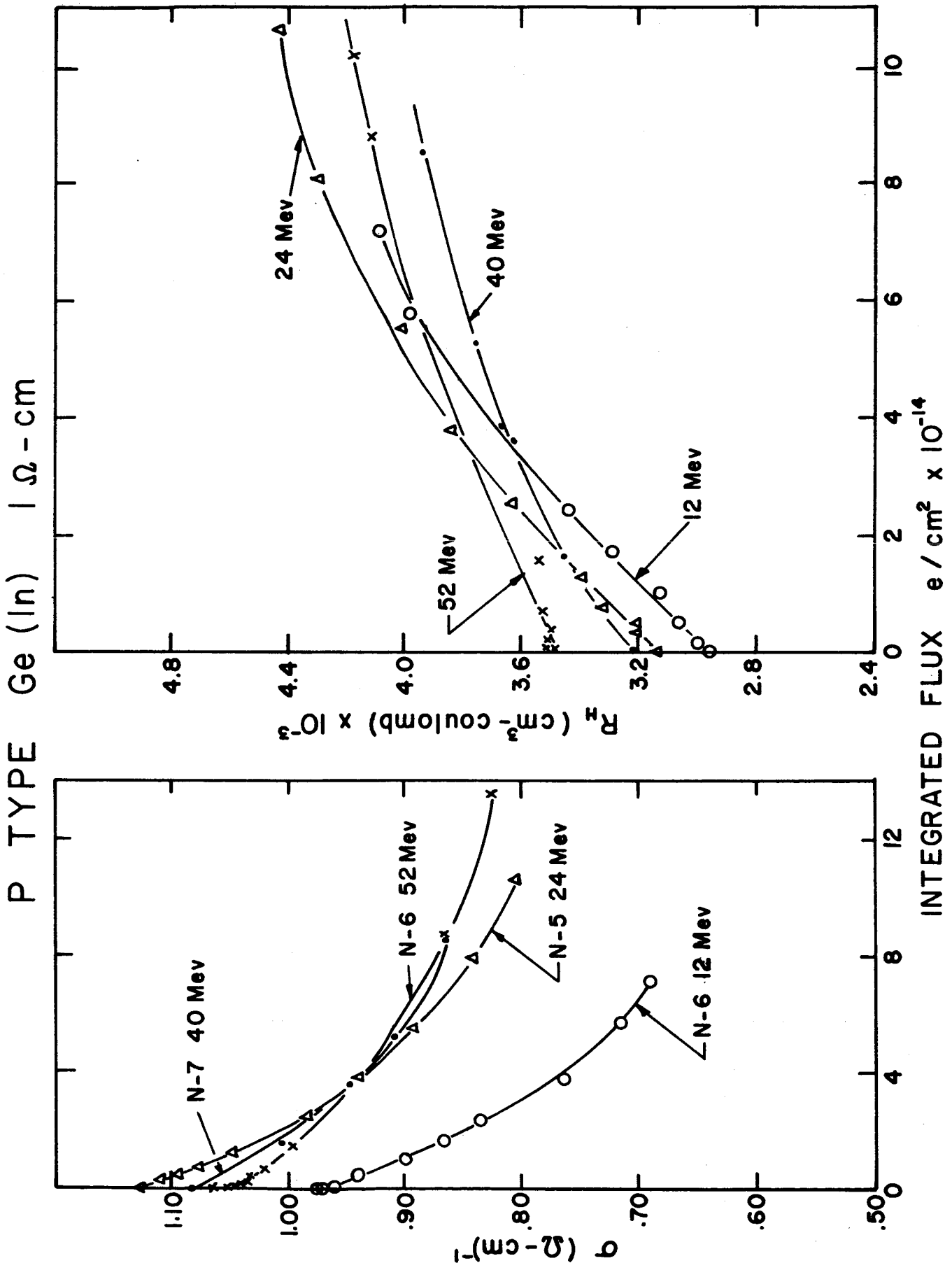
P TYPE Ge (In) 1 Ω - cm
24 Mev
40 Mev
12 Mev
52 Mev
$R_H$ ($cm^3$-coulomb) x $10^{-3}$
INTEGRATED FLUX e / $cm^2$ x $10^{-14}$
N-7 40 Mev
N-6 52 Mev
N-5 24 Mev
N-6 12 Mev
σ ($\Omega$-cm)$^{-1}$

Figure 16

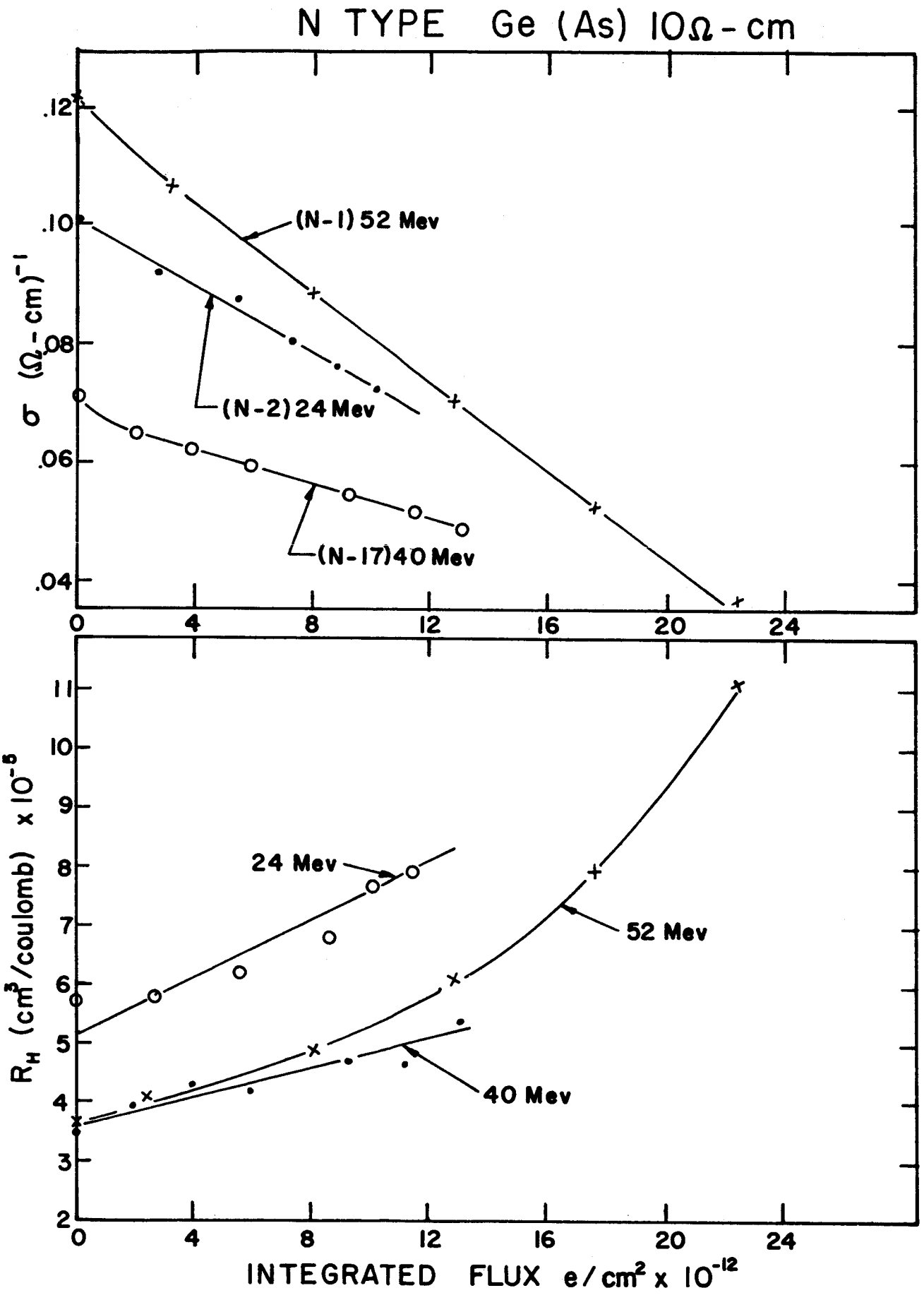
N TYPE Ge (As) 10Ω - cm
σ (Ω - cm)⁻¹
.12
.10
.08
.06
.04
(N-1) 52 Mev
(N-2) 24 Mev
(N-17) 40 Mev
0
4
8
12
16
20
24
R_H (cm³/coulomb) x 10⁻⁶
11
10
9
8
7
6
5
4
3
2
24 Mev
52 Mev
40 Mev
INTEGRATED FLUX e/cm² x 10⁻¹²

Figure 17

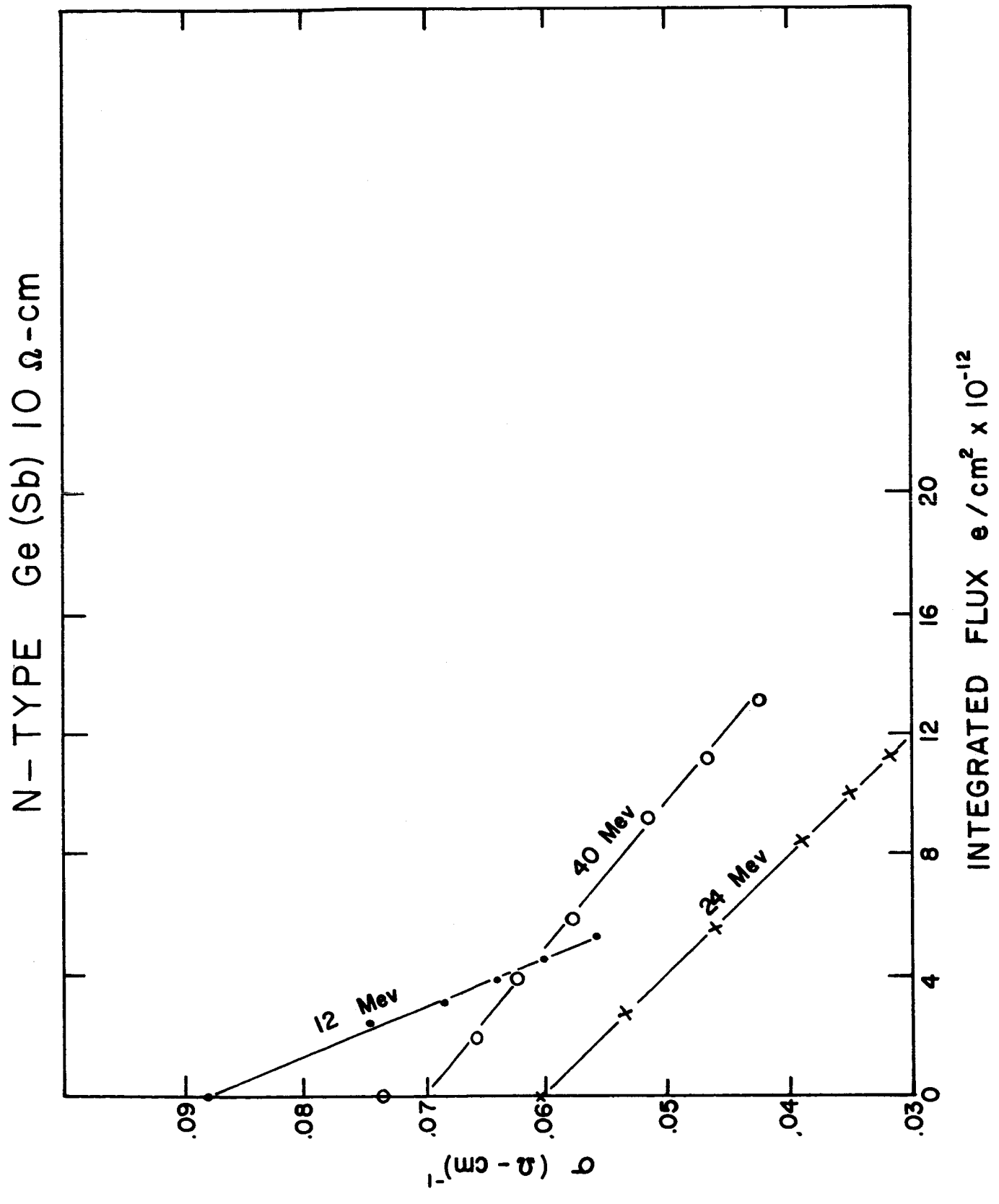
N-TYPE Ge (Sb) 10 Ω-cm
σ (Ω-cm)⁻¹
.09
.08
.07
.06
.05
.04
.03
INTEGRATED FLUX e/cm² x 10⁻¹²
0
4
8
12
16
20
12 Mev
40 Mev
24 Mev

Figure 18

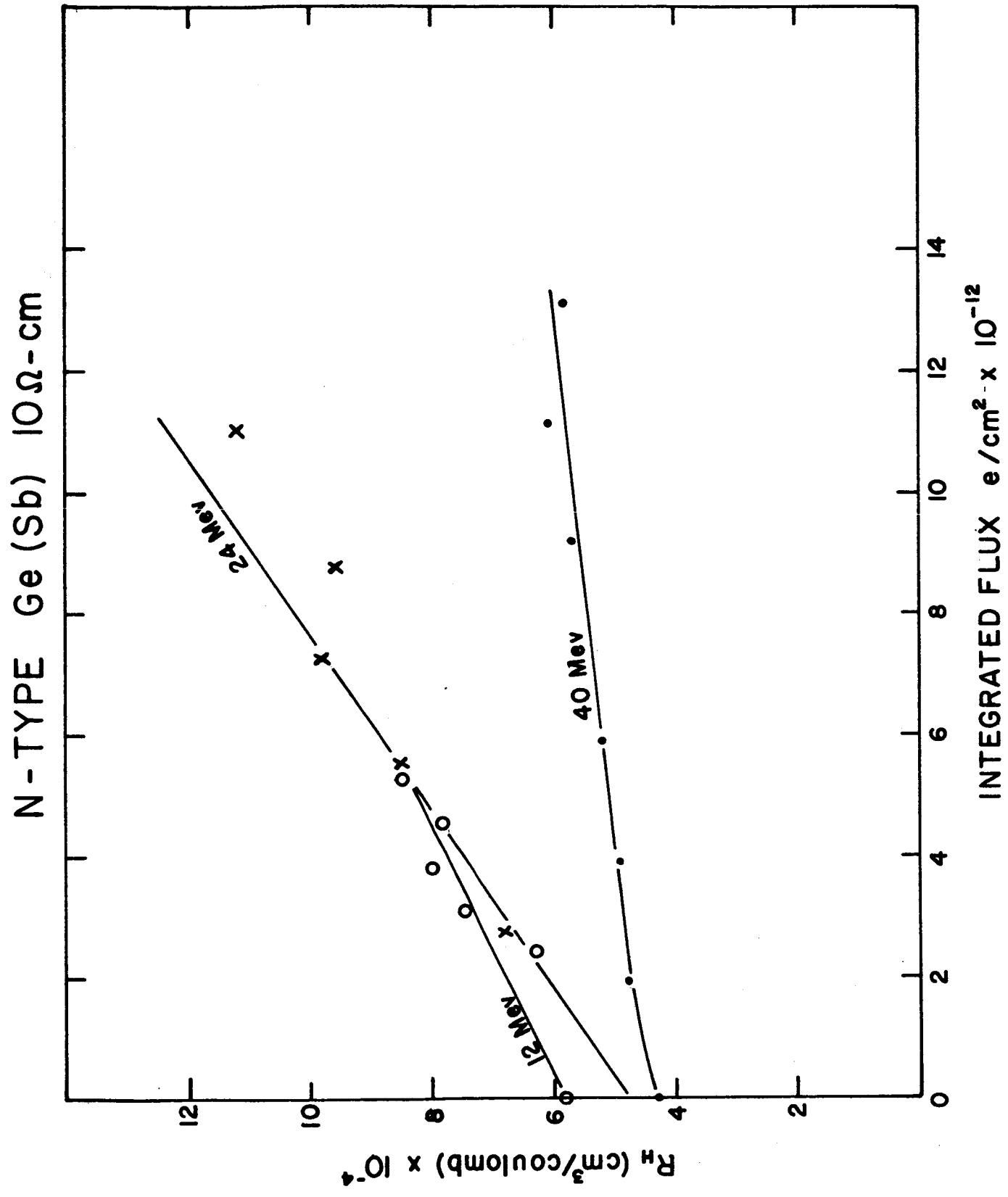
N-TYPE Ge (Sb) 10Ω-cm
$R_H$ (cm³/coulomb) x $10^{-4}$
INTEGRATED FLUX e/cm² x $10^{-12}$
0
2
4
6
8
10
12
14
24 Mev
40 Mev
12 Mev

Figure 19

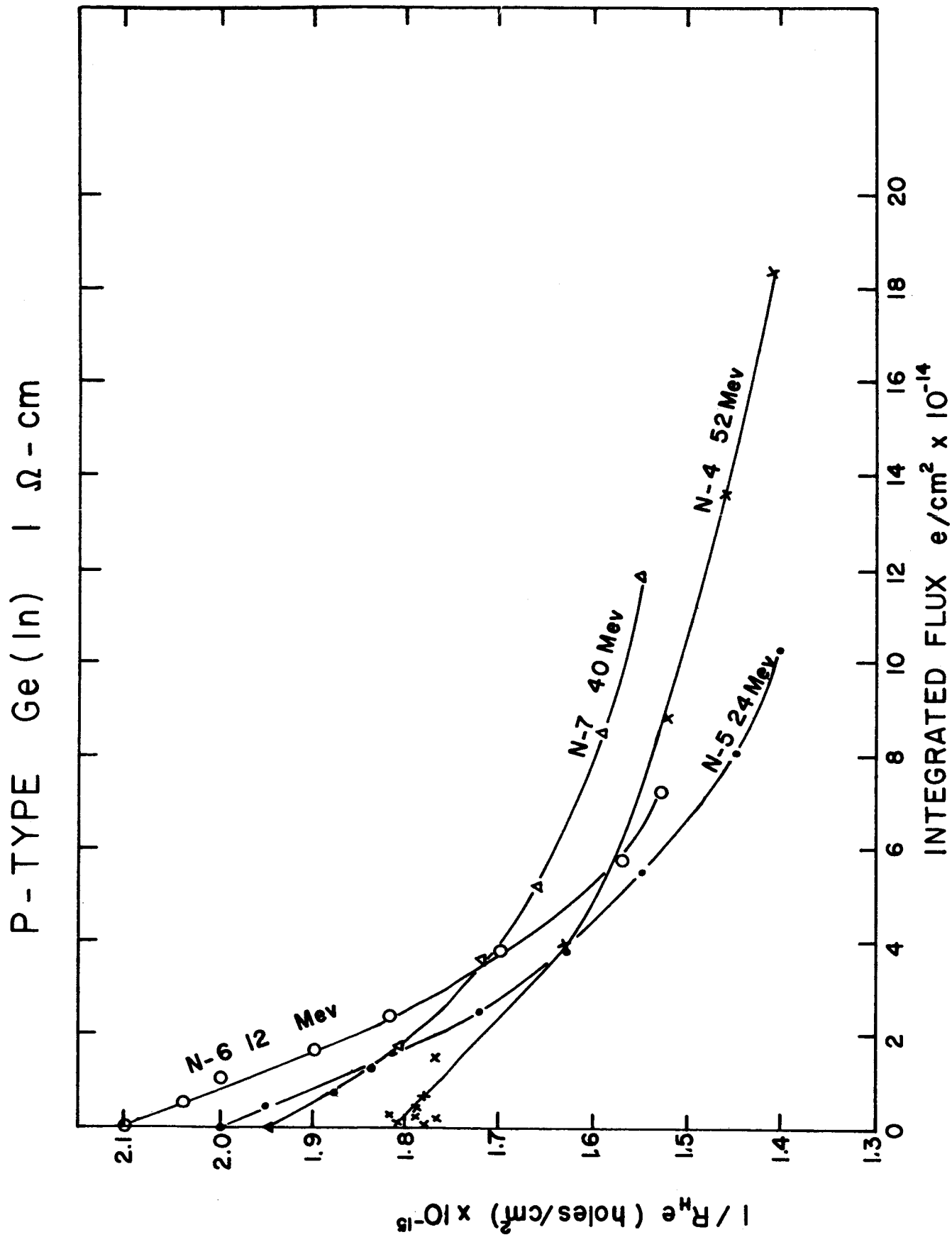
P-TYPE Ge (In) 1 Ω-cm
N-6 12 Mev
N-7 40 Mev
N-4 52 Mev
N-5 24 Mev.
INTEGRATED FLUX e/cm² x 10⁻¹⁴
1 / RHe (holes/cm³) x 10⁻¹⁵
2.1
2.0
1.9
1.8
1.7
1.6
1.5
1.4
1.3
0
2
4
6
8
10
12
14
16
18
20

Figure 20

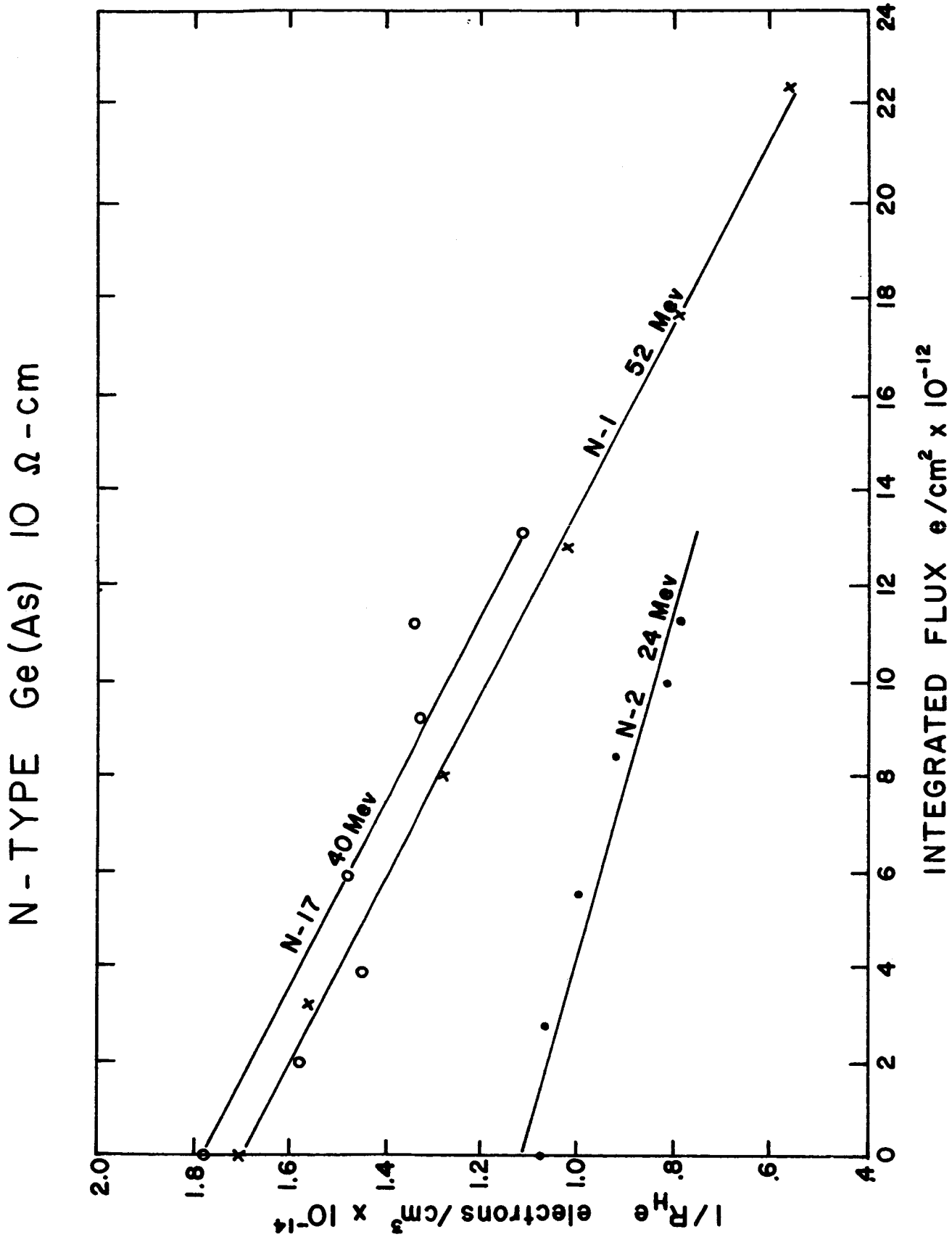
N-TYPE Ge(As) 10 Ω-cm
N-17 40 Mev
N-1 52 Mev
N-2 24 Mev
1/R_He electrons/cm³ x 10⁻¹⁴
INTEGRATED FLUX e/cm² x 10⁻¹²
2.0
1.8
1.6
1.4
1.2
1.0
.8
.6
.4
0
2
4
6
8
10
12
14
16
18
20
22
24

Figure 21

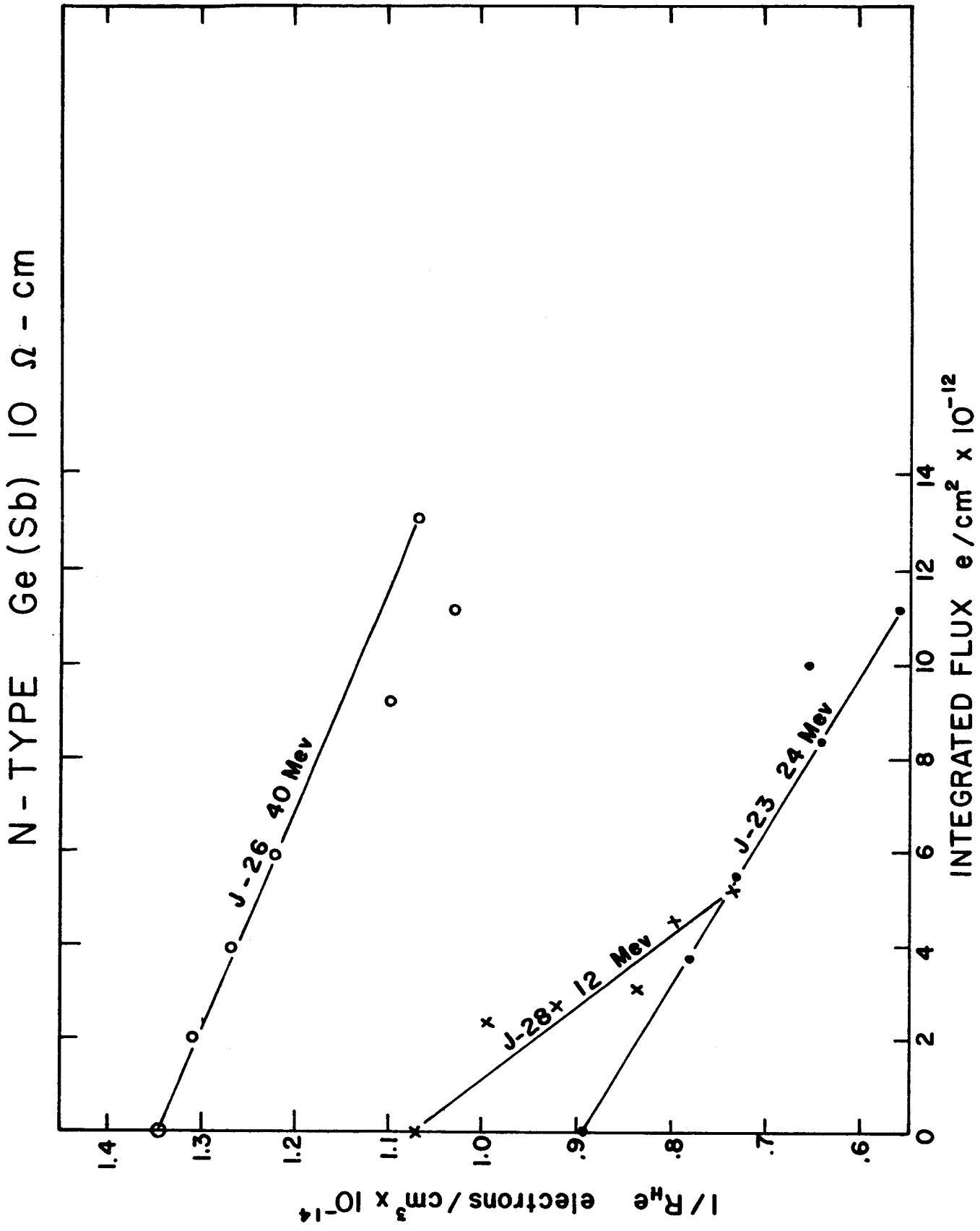
N-TYPE Ge(Sb) 10 Ω - cm
J-26 40 Mev
J-28+ 12 Mev
J-23 24 Mev
1/R_He electrons/cm³ x 10⁻¹⁴
INTEGRATED FLUX e/cm² x 10⁻¹²
1.4
1.3
1.2
1.1
1.0
.9
.8
.7
.6
0
2
4
6
8
10
12
14

Figure 22

# CARRIER REMOVAL RATES

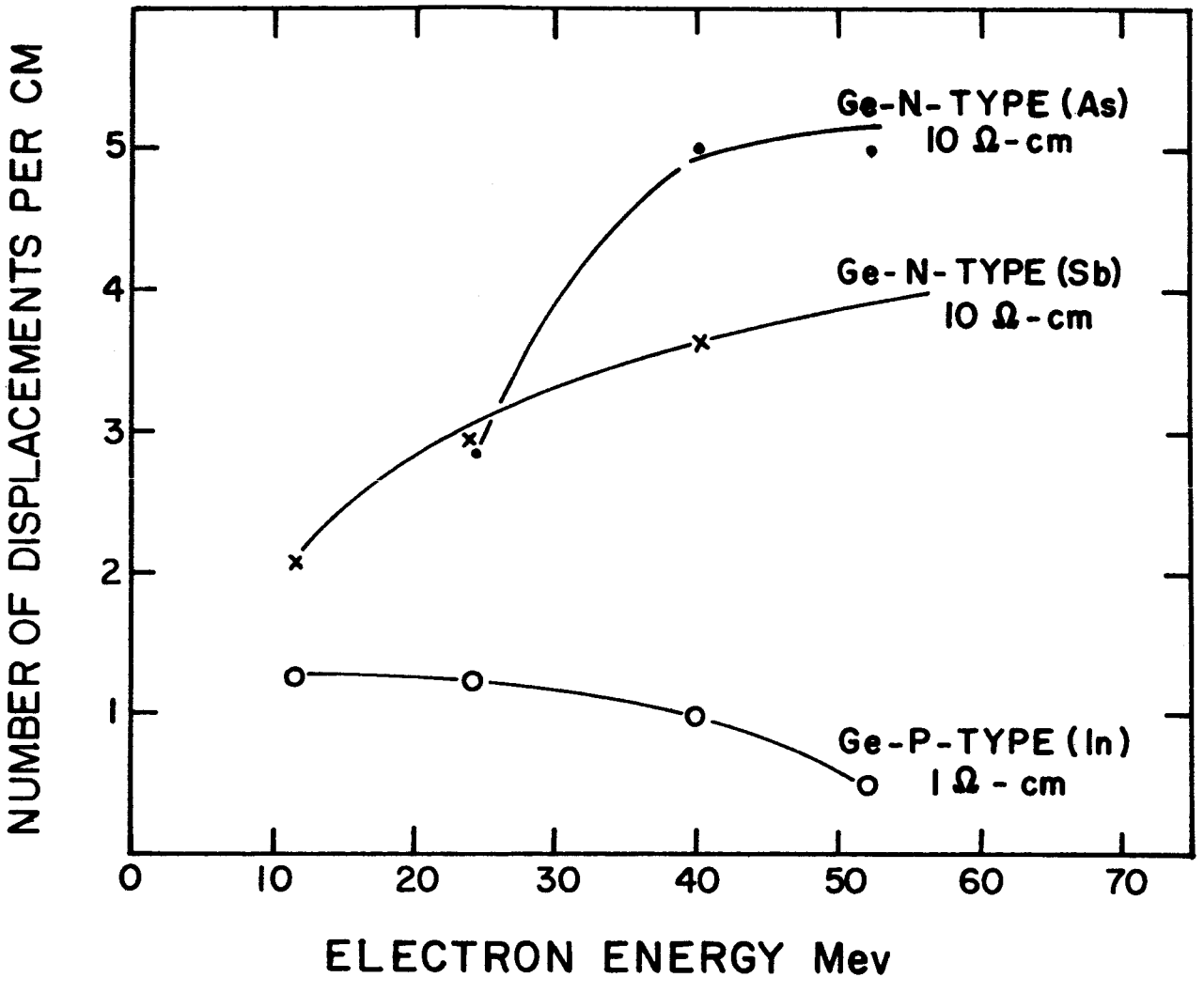


Figure 23

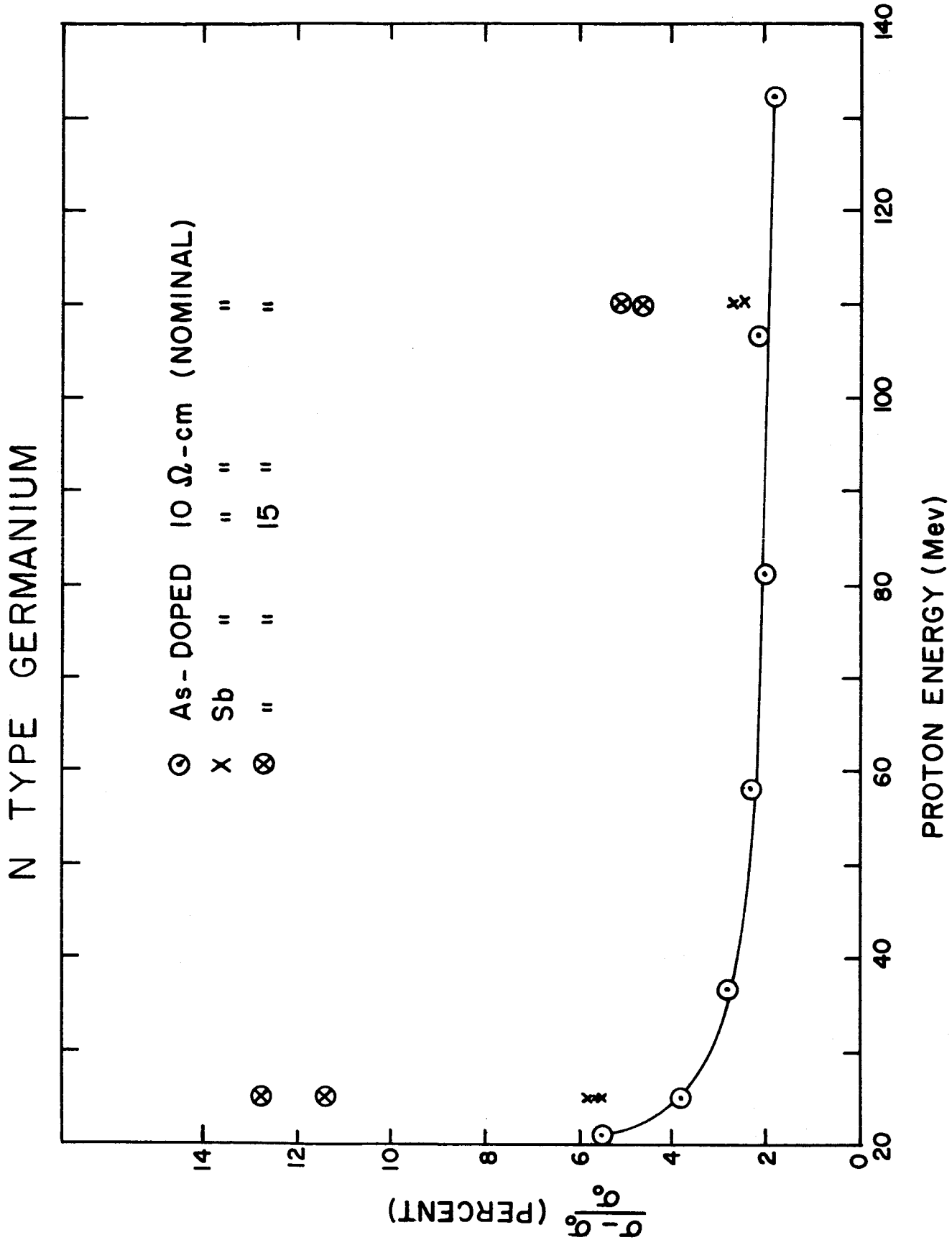
N TYPE GERMANIUM
As- DOPED 10 Ω-cm (NOMINAL)
Sb " 15 "
" "
" "
PROTON ENERGY (Mev)
(PERCENT)
0
2
4
6
8
10
12
14
20
40
60
80
100
120
140

Figure 24

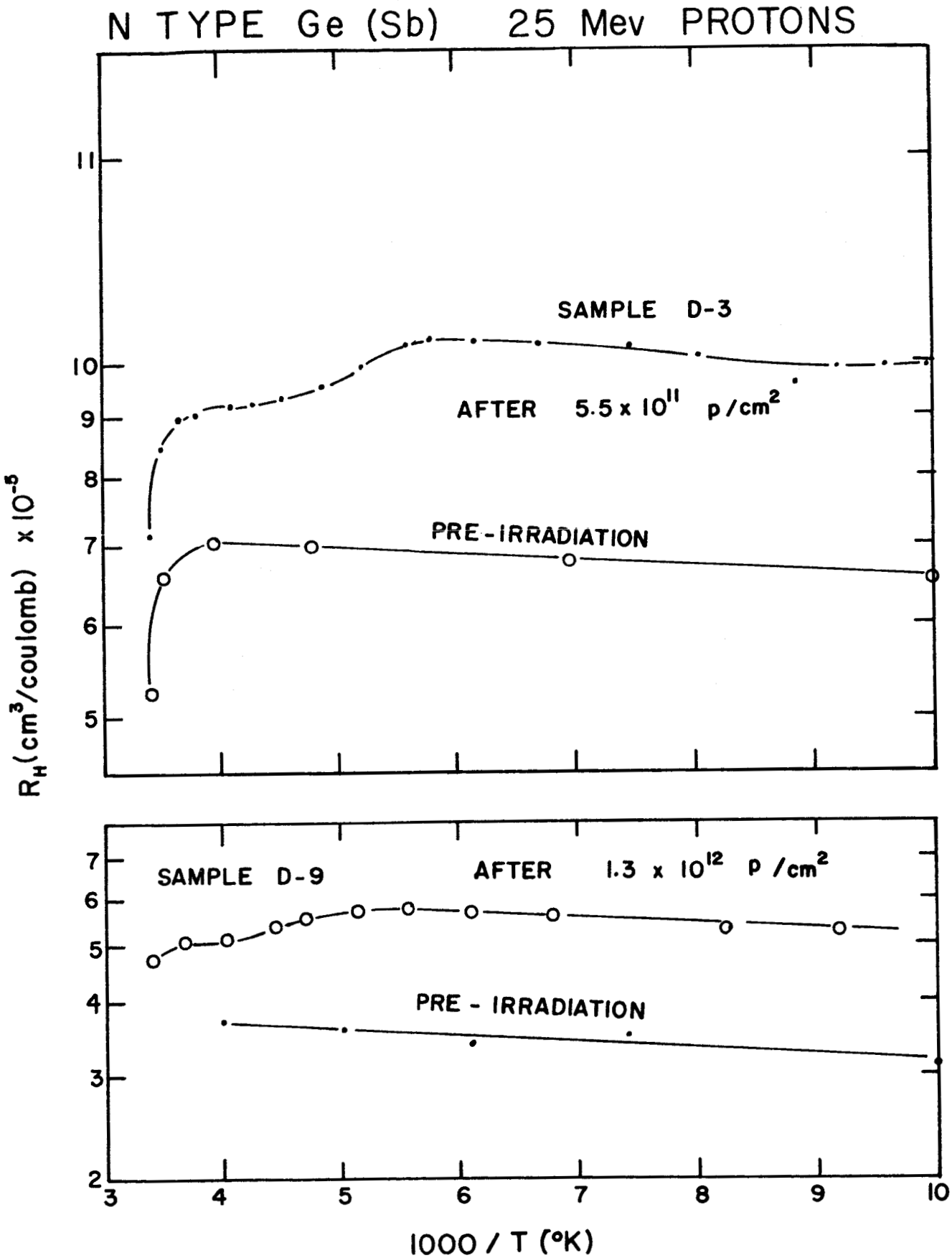
N TYPE Ge (Sb) 25 Mev PROTONS
SAMPLE D-3
AFTER 5.5 x 10^11 p/cm^2
PRE-IRRADIATION
SAMPLE D-9
AFTER 1.3 x 10^12 p/cm^2
PRE - IRRADIATION
R_H (cm^3/coulomb) x 10^-5
1000 / T (°K)

Figure 25